

Quality control by THz spectroscopy of animal feeds and a printed polarizer

by

Marjan MANSOURIAN

THESIS PRESENTED TO ÉCOLE DE TECHNOLOGIE SUPÉRIEURE
IN PARTIAL FULFILLMENT OF THE MASTER'S DEGREE
WITH THESIS IN ELECTRICAL ENGINEERING
M.A.Sc.

MONTREAL, APRIL 18, 2022

ÉCOLE DE TECHNOLOGIE SUPÉRIEURE
UNIVERSITÉ DU QUÉBEC



Marjan Mansourian, 2022



This Creative Commons license allows readers to download this work and share it with others as long as the author is credited. The content of this work cannot be modified in any way or used commercially.

BOARD OF EXAMINERS

THIS THESIS HAS BEEN EVALUATED
BY THE FOLLOWING BOARD OF EXAMINERS

Mr. François Blanchard, Thesis Supervisor
Department of Electrical Engineering, École de technologie supérieure

Mr. Ricardo Izquierdo, President of the Board of Examiners
Department of Electrical Engineering, École de technologie supérieure

Mr. Claude Thibault, Member of the jury
Department of Electrical Engineering, École de technologie supérieure

THIS THESIS WAS PRESENTED AND DEFENDED
IN THE PRESENCE OF A BOARD OF EXAMINERS AND PUBLIC
ON APRIL 5, 2022
AT ÉCOLE DE TECHNOLOGIE SUPÉRIEURE

ACKNOWLEDGMENT

Firstly, I would like to express my gratitude to my patient and supportive supervisor, professor François Blanchard, who has supported me throughout this research project. I am incredibly grateful for his guidance during the running of this project.

Furthermore, I would also like to appreciate my spouse; his pure love and support made my path more convenient.

Also, I cannot forget to thank my family for all the unconditional support. They always encourage me throughout my whole life to reach my goals.

To conclude, I want to thank Xavier Ropagnol, especially for his help and support, and my friends at the LACIME laboratory.

Contrôle de la qualité par spectroscopie THz des aliments pour animaux et d'un polariseur imprimé

Marjan MANSOURIAN

RÉSUMÉ

Ce projet de master vise à fournir des applications de la spectroscopie THz dans le contrôle et l'inspection de la qualité. La revue de la littérature se concentre sur les ondes THz et explique les différents aspects de la spectroscopie THz, en mettant l'accent sur le contrôle de la qualité des aliments. En outre, pour faciliter la compréhension de la spectroscopie THz et de ses possibilités en matière de contrôle de la qualité, l'utilisation des ondes THz est définie dans le contexte de la fabrication de produits électroniques imprimés (PE). La section méthodologie comprend trois configurations différentes pour l'inspection des aliments par spectroscopie THz et la préparation des échantillons pour cette étude. Pour mieux comprendre la spectroscopie THz par réflexion, quatre échantillons différents sont étudiés par simulation de réflexion. Enfin, la fonctionnalité d'un polariseur térahertz (THz) fabriqué à l'aide d'une presse à rouleaux industrielle pour imprimer de l'encre à nanoparticules d'argent sur du polyéthylène téréphtalate (PET) a été étudiée par spectroscopie THz dans le domaine temporel. Les résultats confirment la différenciation du signal entre l'échantillon de plastique à 0% et l'échantillon contenant 20% de volume de plastique. L'identification des fréquences qui peuvent être utilisées pour ce type d'inspection est assez claire. La gamme de fréquences entre 0,2 et 0,4 THz semble être la candidate parfaite pour sonder l'alimentation. Enfin, en regardant les résultats du polariseur fabriqué, tous les degrés symétriques se soutiennent mutuellement, confirmant le bon fonctionnement du polariseur. Un empilement supplémentaire de ces polariseurs bon marché démontre des performances presque équivalentes à celles des polariseurs commerciaux dans la gamme de fréquences de 0,1 à 1 THz.

Mots-clés: Spectroscopie THz, Inspection des aliments, Polariseur

Quality control by THz spectroscopy of animal feeds and a printed polarizer

Marjan MANSOURIAN

ABSTRACT

This master's project aims to provide applications of THz spectroscopy in quality control and inspection. The literature review focuses on THz waves and explains the different aspects of THz spectroscopy, with emphasis on food quality control. In addition, to facilitate the understanding of THz spectroscopy and its possibilities for quality control, the use of THz waves is defined in the context of printed electronics (PE) manufacturing. The methodology section includes three different configurations for THz spectroscopy food inspection and sample preparation for this study. To better understand THz reflection spectroscopy, four different samples are studied by reflection simulation. Finally, the functionality of a terahertz (THz) polarizer fabricated using an industrial roller press to print silver nanoparticle ink on polyethylene terephthalate (PET) was investigated by THz time domain spectroscopy.

The results confirm the differentiation of the signal between the 0% plastic sample and the sample containing 20% plastic volume. The identification of frequencies that can be used for this type of inspection is quite clear. The frequency range between 0.2 and 0.4 THz seems to be the perfect candidate for probing feed. In addition, the results of the reflection simulation show that wavelet analysis could be a good tool for detecting minor particle features. Finally, looking at the results of the fabricated polarizer, all symmetric degrees support each other, confirming the proper functioning of the polarizer. Further stacking of these inexpensive polarizers demonstrates nearly equivalent performance of commercial polarizers in the 0.1 to 1 THz frequency range.

Keywords: THz Spectroscopy, Food inspection, Polarizer

TABLE OF CONTENTS

	Page
INTRODUCTION	1
CHAPTER 1 LITERATURE REVIEW	7
1.1 Introduction	7
1.2 THz radiation	7
1.3 THz applications	10
1.3.1 Biomedical applications of THz spectroscopy	11
1.3.2 Safety and security applications of THz spectroscopy	12
1.3.3 Agriculture applications of THz spectroscopy	12
1.3.4 Food industry applications of THz spectroscopy.....	13
1.4 Food industry challenges.....	17
1.5 Printed Electronic (PE).....	18
1.5.1 Printable electronic material	21
1.5.1.1 Functional ink	21
1.5.1.2 Substrate.....	21
1.6 Existing printing methods	22
1.7 THz waves and printed electronics	23
CHAPTER 2 METHODOLOGY	27
2.1 Introduction	27
2.2 THz Time -Domain Spectroscopy (THz-TDS).....	27
2.2.1 THz-TDS system	28
2.2.2 Emission and detection of THz radiation.....	29
2.2.2.1 Terahertz generation by PCA.....	29
2.2.2.2 Terahertz detection.....	31
2.3 THz-TDS technique	32
2.3.1 Transmission mode	33
2.3.2 Reflection mode	35
2.4 Experimental setup for powder spectroscopy	38
2.5 Experimental setup for printed polarizer	37
2.6 Sample preparation.....	38
2.7 Reflection simulation	43
CHAPITRE 3 RESULTS AND ANALYSIS	47
3.1 Introduction	47
3.2 Animal food powder results	47
3.3 Reflection simulation results	56
3.4 Polarizer quality control results.....	60
CONCLUSION AND RECOMMENDATIONS	69

APPENDIX I	SAMPLE HOLDER.....	71
APPENDIX II	WAVELET ANALYSIS IN DIFFERENT SAMPLES.....	73
BIBLIOGRAPHY	75

LIST OF TABLES

	Page
Table 1.1	Comparison of traditional vs printable electronics20
Table 2.1	Weight of all samples.....42

LIST OF FIGURES

		Page
Figure 1.1	The electromagnetic spectrum. The THz band lies between microwave and infrared	8
Figure 1.2	The various molecular interactions in the terahertz frequency region	10
Figure 1.3	THz spectroscopy and imaging applications	11
Figure 1.4	Photos of each sample, (a)80, (b)40, (c)10, and (d)1 hair.	14
Figure 1.5	Terahertz spectrum of turmeric mixed with different concentrations of chalk powder	15
Figure 1.6	Absorbance spectra containing different kinds of TCH in infant milk powder with a zoom view in the inset.....	16
Figure 1.7	Application areas of flexible and printed electronics	19
Figure 1.8	A schematic diagram of flexography printing	22
Figure 1.9	An image of the 40 μm gap, 40 μm width wire grid polarizer with four layers (40G/40W/4L)	24
Figure 1.10	Transmission imaging measurement of a printed meander-line pattern by THz-TDS. Left: images at selected frequencies; Right: permittivities and loss tangents at selected points	26
Figure 2.1	Diagram of a THz TDS spectrometer in transmission geometry. A beam splitter divides the ultrashort pulse. A mirror guides one part to the transmitter for terahertz generation, and the other part is guided by a set of mirrors through the delay line and then to the receiver for terahertz detection.....	28
Figure 2.2	Terahertz generation by a photoconductive antenna	31
Figure 2.3	Terahertz detection by a photoconductive antenna.....	32
Figure 2.4	Geometry for Electric Field Transmission of incident waves with amplitude E through a layer of thickness d with refractive index n_2	33

Figure 2.5	Reflection geometry for complex-response measurement in a sample with thickness d	36
Figure 2.6	Terahertz Time-Domain setup	37
Figure 2.7	A visible image of a printed polarizer.....	38
Figure 2.8	a; THz-TDS system ,b; THz-TDS system with one lens, c; THz-TDS system with two lenses.....	39
Figure 2.9	Sample holder	40
Figure 2.10	Measurement of the empty sample box with a digital scale	41
Figure 2.11	Animal food samples	43
Figure 2.12	Reflection spectroscopy set-up	44
Figure 2.13	Sample with 33% plastic and Aluminum(AL).....	45
Figure 2.14	Reflection simulation with a sample.....	46
Figure 3.1	Samples THz-TDS	48
Figure 3.2	Time-domain spectra of samples zoom image.....	49
Figure 3.3	THz Frequency Domain.....	50
Figure 3.4	THz frequency domain zoomed image	51
Figure 3.5	Time- Domain Spectra of samples when one lens add.....	52
Figure 3.6	Zoomed image of Time-domain spectra of samples.....	52
Figure 3.7	THz Frequency domain of samples when the one lens add.....	53
Figure 3.8	Time- Domain Spectra of samples when the two lenses add.....	54
Figure 3.9	Zoomed image of Time-domain spectra of samples when the two lenses add.....	55
Figure 3.10	THz Frequency domain of samples when the two lenses added	56
Figure 3.11	Different samples THz-TDS	57
Figure 3.12	THz Time-Domain Spectroscopy of a) sample 1 and b) sample 2	58
Figure 3.13	Sample 1 wavelet analysis	59

Figure 3.14	Sample 2 wavelet analysis	60
Figure 3.15	Normalized amplitude of Horizontal and Vertical polarizer position.....	61
Figure 3.16	THz-TDS of polarizer in different positions.....	62
Figure 3.17	THz-TDS of polarizer in different positions	62
Figure 3.18	Normalized amplitude of different polarizer position	63
Figure 3.19	Normalized amplitude as a function of angels.....	64
Figure 3.20	Normalized amplitude as a function of angels.....	65
Figure 3.21	Extinction ratio of one layer polarizer and two layer polarizer	66
Figure 3.22	evolution of the skin depth of printed silver metal as a function of frequency	67

LIST OF ABBREVIATIONS

EM	Electro-Magnetic
EO	Electro-Optic
FFT	Fast-Fourier Transform
MMs	Metamaterials
NIR	Near-Infrared
PCA	Photo-Conductive Antenna
PET	Polyethylene Terephthalate
PE	Printed Electronics
R2R	Roll-to-Roll
THz	Terahertz
TDS	Time Domain Spectroscopy
UV	Ultraviolet

INTRODUCTION

The way food is produced and distributed has fundamentally changed over the past few decades. As a result, food security has become more complex, driven by the widespread use of food production and processing methods, linked to the rapid increase in the global food trade. In addition, food processing is becoming more automated, significantly increasing the speed and volume of production. On the other hand, food safety risks are increasing due to globalization and changes in the food industry. Therefore, the food industry must employ processing techniques to ensure product quality and safety (Arduini, Cinti, Scognamiglio, & Moscone, 2016).

Traditional methods such as polymerase chain reaction (Okuma & Hellberg, 2015), chromatography methods (Manzi & Pizzoferrato, 2013), and enzyme-linked immunosorbent assay (Santiago-Felipe, Tortajada-Genaro, Puchades, & Maquieira, 2014) are available for analysis in food and the environment. These techniques are complex, expensive, and time-consuming. Therefore, the industry needs to develop simple, accurate, rapid, nondestructive, and in-situ methods to evaluate food products. In recent years, different spectroscopy and imaging methods have been attempted and developed for qualitative and quantitative analysis of several compounds (Haughey, Galvin-King, Ho, Bell, & Elliott, 2015), (Liu, Sun, & Zeng, 2014) such as Raman spectroscopy (Lee & Herrman, 2016), Near-Infrared (NIR) spectroscopy (Catelani et al., 2017), magnetic resonance imaging (Bao et al., 2017), X-ray imaging (J. L. Li, Sun, & Cheng, 2016), etc. Recently, a new emerging spectroscopy technique, namely Terahertz (THz) spectroscopy, has been (Guerboukha, Nallappan, & Skorobogatiy, 2018) tried to detect contaminants inside food products.

THz radiation generally refers to electromagnetic waves with frequencies between 0.1 and 10 THz ($3 \text{ mm} > \lambda > 30 \text{ }\mu\text{m}$), which is between the mid-infrared and microwave ranges (Zhang & Xu, 2010). Due to their non-destructive property, terahertz waves can be safely used for food process monitoring and quality control (Corsi & Sizov, 2014). Studies show that many physical phenomena, such as vibrational modes, including the rotational and vibrational energy levels of many biomolecules (e.g., proteins and DNA), are in the terahertz frequency range. In

addition, terahertz frequency provides valuable information about intramolecular and intermolecular modes related to weak and conformational interactions, including hydrogen bonding and the Van der Waals force in various chemical materials (Baxter & Guglietta, 2011). In addition, compared to the optical and near-infrared spectra used, the wavelength of the terahertz spectral range is longer and thus will not be affected by scattering (Lu, Zhang, Zhang, Yang, & Xiang, 2016). Due to the specific characteristics of THz waves, several studies have demonstrated the potential of THz quality control in different aspects of the food industry, such as foreign body detection, determination of pesticides and antibiotics, and detection of toxic compounds (Baek et al., 2016), and (Afsah-Hejri, Hajeb, Ara, & Ehsani, 2019).

Another major problem of modern society is the overuse of antibiotics in industrial animal husbandry, which in the end can be swallowed by humans. Food-borne antibiotics are a serious health risk, and the overuse of antibiotics affects human health, such as toxic and allergic reactions. (Massaouti, Daskalaki, Gorodetsky, Koulouklidis, & Tzortzakis, 2013). THz spectroscopy has been shown to be able to detect tetracycline hydrochloride (TCsH) in infant milk powder. Tetracycline (TCs) is a widely used antibiotic in milk and meat products (Qin, Xie, & Ying, 2014).

Fraud in the food industry is common and food adulteration is a major food safety concern (Y. Cui, Mu, Wang, Zhang, & Zhang, 2009). For example, melamine is a nitrogen-rich molecule with 40% nitrogen by atomic number. Because of its high nitrogen content, this chemical is illegally added to foods such as milk powder to increase the total nitrogen concentration, which is used as an indicator to assess protein content. Melamine ingestion by pets, livestock and infants leads to serious health problems associated with the reproductive system and kidneys. In 2014, a group of researchers investigated the feasibility of detecting melamine in food by terahertz spectroscopy. Different absorption peaks of melamine at 2, 2.26, and 2.6 THz were observed in all food mixtures, and at 2 THz, detected THz image of melamine was dose-dependent (Baek et al., 2014).

Another problem is the presence of foreign bodies, such as plastic, stones, glass, fingernails, hair and even insects in food products during the packaging process (Haff & Toyofuku, 2008). The presence of insects in nuts is common and is one of the problems affecting nut quality.

Usually, infected nuts are cleaned by a mechanical cleaning method of floating them in a chemical solution and picking them up by hand under ultraviolet (UV) lamps (Tan, Lu, Luo, & Xie, 2014). This technique is expensive and inefficient. Li et al. (2010) successfully detected dead and live insects in pecans based on their water content and differences in absorption coefficient in the THz region (Li, Cao, Mathanker, Zhang, & Wang, 2010).

Despite the difficulties in developing efficient sources and detectors for a very long time, the last two decades have seen the emergence of powerful and efficient sources and detectors. The emergence of these new sources and detectors has given impetus to the development of new techniques applied to characterization, spectroscopy, and imaging in the near future, to telecommunications (Guerboukha et al., 2018).

From an optics/photonics perspective, the photon energy of the THz wave is much lower than that of visible and near-infrared light, and, therefore, it is not easy to control and manipulate the THz wave. For example, the development of THz time-domain spectroscopy (THz-TDS) (Grischkowsky, Keiding, Van Exter, & Fattinger, 1990) and (Davies & Linfield, 2003) has advanced the state of the art. More recently, artificially structured electromagnetic (EM) materials have become a particularly active area of research due to the ability to create materials that exhibit novel EM responses not available in natural materials (Smith, Pendry, & Wiltshire, 2004). These composites, often referred to as metamaterials (MMs), are sub-wavelength composites, where the EM response comes from the oscillation of electrons in significantly conductive metals such as gold or copper, allowing for a particular resonant response of electrical permittivity or magnetic permeability (Liu, Ji, Mock, Cui, & Smith, 2008). MMs are essential for the technologically relevant the THz frequency regime to create a new component for manipulating these wave (Veselago, 1968). The downside of these materials is the technical difficulty and cost of their fabrication, as most approaches are complex and require high-tech instrumentation in an expensive clean room environment (Tao, Padilla, Zhang, & Averitt, 2010). It is only recently that additive manufacturing has paved the way for the development of such low-cost metasurfaces and has even shown promising

possibilities for controlling the quality of materials or a manufacturing process (Zhuldybina, Ropagnol, Bois, Zednik, & Blanchard, 2020)

Thesis objectives

In this study, we used the non-destructive nature of THz waves to test dry dog food for plastic contaminants. The combination of non-destructive penetration and the unique spectral characteristics of many substances makes THz radiation very suitable for food inspection applications. This study examined the possibility of detecting and identifying harmful contaminants such as plastic particles in dog food using THz spectroscopy.

Since spectroscopy of a powdered sample is a rather difficult task, my first task was to learn THz spectroscopy using a simpler and more standard sample. Therefore, during my master's degree, I performed spectroscopy of a THz polarizer printed from a printable electronics (PE) fabrication method of fabrication. The results show that such devices are promising for working at THz frequencies and less expensive to produce.

Thesis organization

This thesis is organized into four different chapters as follows:

Chapter one describes the history of THz spectroscopy and its applications in general, focuses on previous work done in the food industry, and then explains the history of PE and other related work.

Chapter Two discusses the source, detectors, and THz time-domain spectroscopy (THz-TDS), and then briefly introduces some of the commonly used THz devices. The evolution the evolution of printable electronics (PE) in the context of THz research is also presented. The final section is devoted to sample preparation. A first part dedicated to the food spectroscopy and which explains the device used for this experiment. A second part details the preparation of the printed polarizer and its design. We conclude with some simulations performed on a THz wave reflection condition for food spectroscopy. This scheme is more realistic for an

industrial environment since it is not always possible to pass through the sample to be inspected.

The third chapter focuses on the results of food spectroscopy in transmission and reflection mode, and then discusses the results of the PE polarizer.

The final chapter presents a summary of this work and possible research directions that could emerge from our results.

Thesis contribution

In this research, we tried to detect contaminants in ground kibble used as dog food as a sample to determine the presence of contaminant using THz-TDS. To our knowledge, this is the first time that food of animal origin has been studied for food inspection with THz spectroscopy. The results clearly show the difference between healthy samples and those with plastic contaminants.

Part of this research which described the fabrication of a THz polarizer is published in IEEE as bellow:

IEEE Publication:

M. Mansourian, M. Zhuldybina, X. Ropagnol, N. D. Trinh, C. Bois and F. Blanchard,
"Fabrication and characterization of a terahertz polarizer from a roll-to
roll printer," *2021 Photonics North (PN)*, 2021, pp. 1-1, doi:
10.1109/PN52152.2021.9597903.

CHAPITRE 1

LITERATURE REVIEW

1.1 Introduction

This chapter describes the properties of THz waves and explains various aspects of the use of THz spectroscopy with emphasis on food quality control. To facilitate the understanding of THz spectroscopy and its possibilities for quality control, we also define the use of THz waves in the context of Printed Electronics (PE) manufacturing.

1.2 THz radiation

The electromagnetic spectrum is the entire range of waves that exists, including microwaves, infrared radiation, visible light, and X-rays. Between the microwave and infrared frequencies, lies the THz waves (see Fig1.1). One THz correspond to a duration of 1 ps, a wavelength of 300 μm , a wavenumber of 33 cm^{-1} , and a photon energy of 4.1 meV. THz radiation, also known as T-rays, makes the bridge between two principal regions: the low frequencies used for electronic communication which are generated and detected mainly by electronic devices and the high frequencies which are mainly generated and detected by optical methods (Shur, 2005). The origin of the THz gap is due to the absence of source and detector of THz radiation for a long period of time. Despite these waves are present naturally in the outer space, they are strongly absorbed by the atmosphere and consequently almost non-existent in our environment. Thus, until the creation of efficient detector, there was no way to detect these waves. In addition, due to the absence of effective sources, it was impossible to generate them "artificially". In the past, infrared and microwave were widely used with the THz gap, completely empty between this two frequency range (Davies & Linfield, 2004). However, in the last four decades, with the development of ultrafast optics, optoelectronic technology, and microscale semiconductor devices, suitable sources and detection methods in the terahertz

band have been reported (Guiramand, Nkeck, Ropagnol, Ozaki, & Blanchard, 2022) (Baxter & Guglietta, 2011; Williams, 2005).

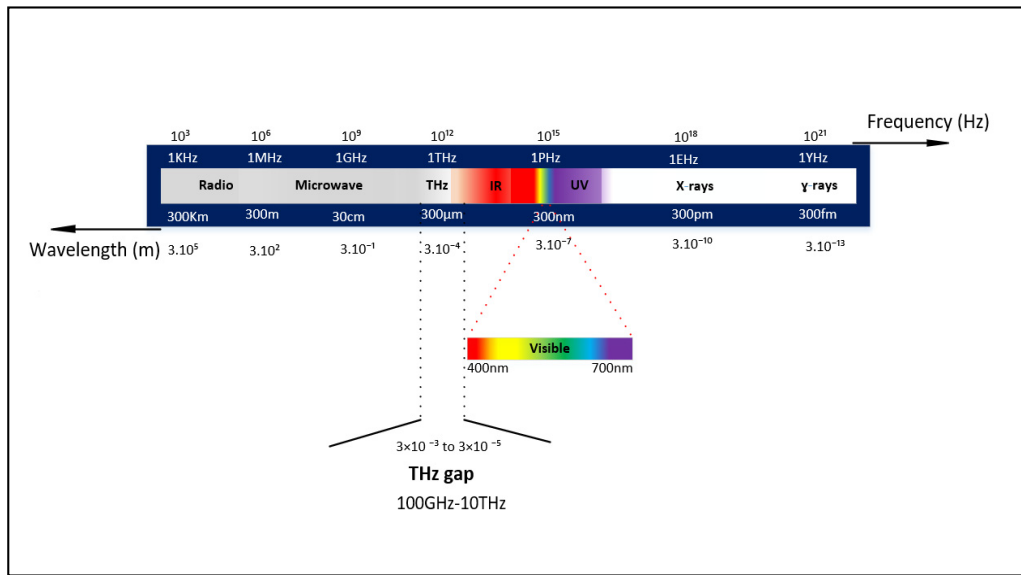


Figure 1.1 The electromagnetic spectrum. The THz band lies between microwave and infrared

1.2.1 THz properties

The unique nature of THz radiation has stimulated researchers to develop this frequency band for several applications. Here are some of the interesting features:

THz radiation is transparent through many non-conductive or optically opaque materials, e.g., polymers, plastic, paper, clothing, wood, and allows inspection of material composition (Jansen et al., 2010; Zhong, 2019). Therefore, by taking advantage of its transparency to clothing and the fact that it is non-hazardous radiation, THz technology can be applied to security operations such as passenger screening in airport terminals (Fan et al., 2017).

THz waves are also strongly absorbed by polar molecules in liquids (such as water) because the hydrogen bond (H - O) within polar molecules resonates strongly in the THz range. For

example, this characteristic is an advantage for monitoring moisture content.(Afsah-Hejri, Hajeb, Ara, & Ehsani, 2019). Concretely, researchers have used this unique property to assess the quality of tomatoes. They showed that trend of decreasing THz reflectivity was found in the damaged area, which may result from moisture loss (Ogawa et al., 2006).

The THz range contains abundant physical and chemical information, as well as many molecular vibrations, including molecular rotations, low-frequency bond vibrations, crystal phonon vibrations, stretching, and hydrogen bond distortions (See Figure 1.2)

(McIntosh, Yang, Goldup, Watkinson, & Donnan, 2012). By measuring the frequency response of the THz band, important information about the structure and response of molecules can be obtained. Absorption spectra thus represent the unique property of the fingerprint of materials (Ueno, Rungsawang, Tomita, & Ajito, 2006).

THz waves have low photon energies. Therefore, it cannot lead to photoionization in biological tissues, as in opposition with X-rays. Thus, THz waves are considered safe for the samples and the operator. Due to high water absorption, THz waves cannot penetrate inside the human body. Hence, even if THz radiations leading to any harm, it is limited to skin level(Afsah-Hejri et al., 2019; Peralta, Lipscomb, Wilminck, & Echchgadda, 2019). THz waves have longer wavelengths than IR and visible waves. It means that THz radiations are few affected by Mie scattering which is the scattered light of particles that have a diameter similar to or larger than the wavelength of the incident light . (Amarasinghe, Zhang, Zhang, Mittleman, & Ma, 2020). Consequently, THz waves are regarded as very promising in nondestructive evaluation applications (Jansen et al., 2010).

The Terahertz technique allows direct measurement of the amplitude and phase of the electric field, which makes it easy to calculate the absorption coefficient and refractive index of the sample. Therefore, the optical parameters can be obtained without using the Kramers-Kronig relation, which is a bidirectional mathematical relations, connecting the real and imaginary

parts of any complex function that is analytic in the upper half-plane and it is a unique advantage over Fourier-Transform Infrared (FTIR) spectroscopy (Gowen, O'Sullivan, & O'Donnell, 2012).

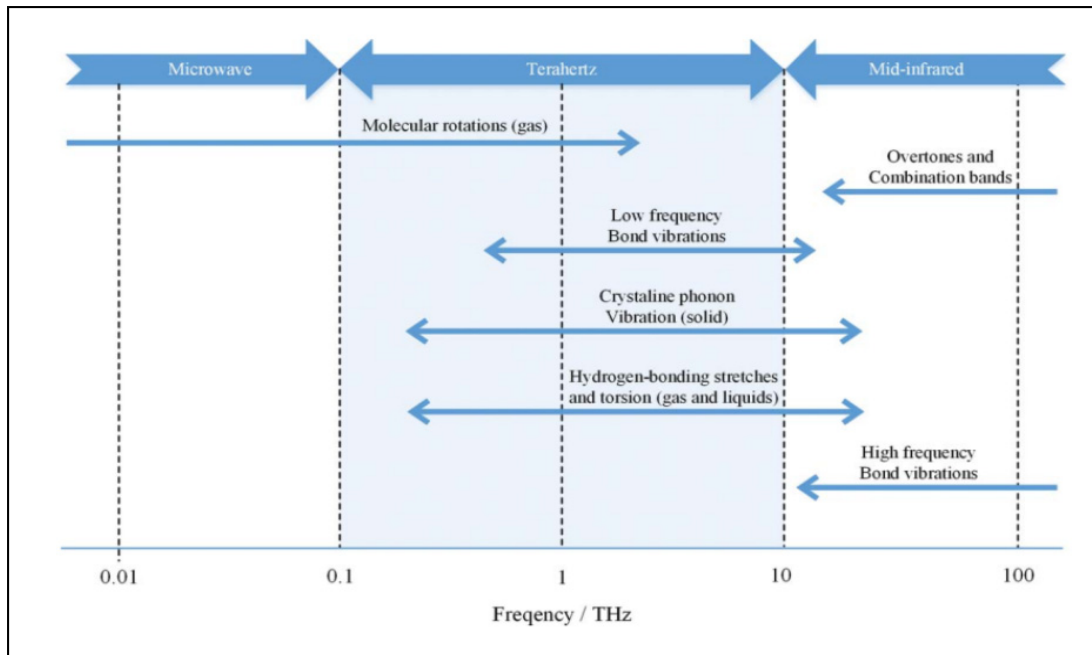


Figure 1.2 The various molecular interactions in the terahertz frequency region
Taken from McIntosh, Yang, Goldup, Watkinson, & Donnan (2012)

1.3 THz applications

After the development of the source and detectors, the next step was the development of applications, which was in fact done in parallel with the development of THz sources and detectors. Due to the unique properties of THz waves, the main application of THz waves is applied spectroscopy for various fields such as biomedical, agriculture, security and food industry (See Figure.3) (Afsah-Hejri et al., 2019). Here are examples of different applications of THz spectroscopy:

1.3.1 Biomedical applications of THz spectroscopy

THz spectroscopy has been used to study many molecules and tissues, including proteins, drugs, cancerous tissues, and DNA (Jin, Zhang, Wu, & Liu, 2010). THz spectroscopy, with its high temporal resolution and high noninvasive sensitivity, can be used to study brain cancer. Yamagushi et al (Yamaguchi et al., 2016) reported that THz reflection spectroscopy was useful for detecting tumor regions in fresh rat brain tissue. The refractive index and absorption coefficient of cancerous tissue were higher than those of normal tissue due to the higher cell density and water content of the cancerous region.

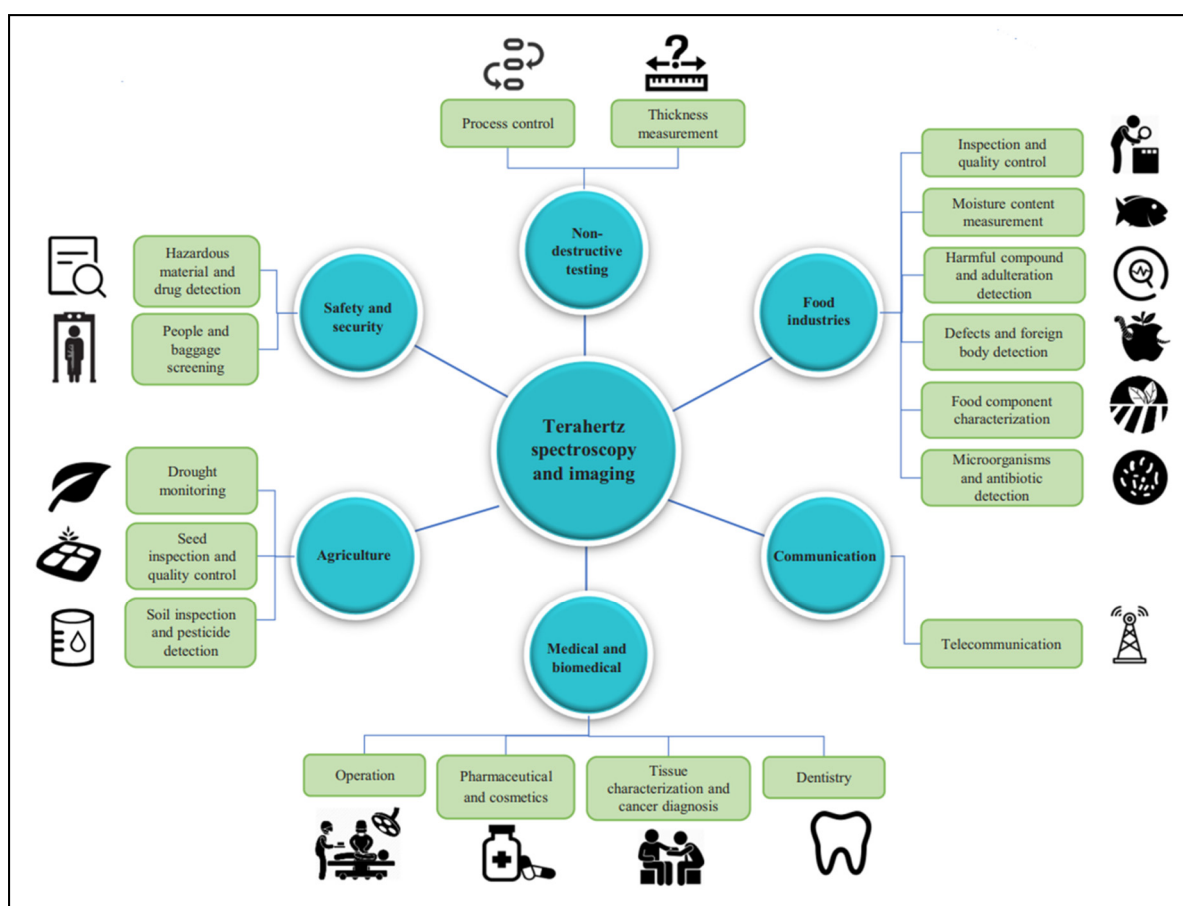


Figure 1.3 THz spectroscopy and imaging applications

1.3.2 Safety and security applications of THz spectroscopy

As mentioned before, THz radiation can penetrate fabrics and plastics. It can therefore be used for screening purposes, such as security checks, to remotely discover hidden weapons on a person (Pawar, Sonawane, Erande, & Derle, 2013). This aspect is exciting because many materials have unique spectral "fingerprints" in the terahertz range. This offers the possibility of combining spectral identification with imaging. Passive detection of terahertz signatures avoids the privacy issues of other types of detection because it is targeted to a particular range of materials and objects (Palka et al., 2012). In airports or other security-critical locations, it is now possible to detect dangerous non-metallic substances, such as ceramic knives or plastic explosives, using terahertz beams. This is possible because T-rays penetrate clothing but cannot penetrate the upper part of the skin (due to its water content) (J. F. Federici et al., 2005).

1.3.3 Agriculture applications of THz spectroscopy

THz spectroscopy has developed rapidly for food safety and quality control over the past two decades. THz spectroscopy has excellent potential for predicting agri-food products, combined with chemometric methods such as principal component analysis, Partial Least Squares (PLS), etc (Ge et al., 2014). For example, wheat is an important agricultural commodity with low insect resistance and antimycotic characteristics and easily sprouts during inadequate post-harvest storage. Therefore, the development of rapid, non-destructive evaluation techniques to maintain safety and reduce losses is of great interest. One study considered different wheat varieties with different nutritional and processing qualities. They discriminated eight wheat varieties subjected to the THz spectroscopy system and showed that the absorption spectrum-based PLS model outperformed the refractive index-based PLS model in predicting wheat varieties in the 0.2 to 1.5 THz range (Ge, Jiang, Lian, Zhang, & Xia, 2015). Detection of toxic compounds in agricultural products is another critical object. For instance, aflatoxin is known to be seriously harmful to humans because it is toxic. Aflatoxin is spread in many agricultural products such as rice, wheat, and soybeans during cultivation, harvest, and storage. THz

spectroscopy with chemometric methods identified aflatoxin in soybean oil with high accuracy (over 90% accuracy) (Liu, Zhao, et al. 2019).

1.3.4 Food industry applications of THz spectroscopy

The food industry has always been important to governments and public opinion because of public health. Due to the increasing demand for food, manufacturers need to develop accurate food monitoring technology to ensure the safety of food products (Afsah-Hejri et al., 2019). The main applications of THz spectroscopy in food industries include moisture detection, foreign body detection, inspection, and quality control (Gowen et al., 2012; Yan, Ying, Zhang, & Yu, 2006). Other applications of THz technology in the food industry include the detection of harmful compounds, antibiotics, and microorganisms (Massaouti, Daskalaki, Gorodetsky, Koulouklidis, & Tzortzakis, 2013; Yang, Yang, Luo, & Fu, 2016). THz spectroscopy is an excellent tool for characterizing carbohydrates, amino acids, fatty acids, and vitamins (Jin et al., 2010; Ueno et al., 2006).

Sometimes small objects fall into food products during the manufacturing process, and it is not easy to see them with the naked eye. In 2013, a group of researchers measured human hair by two orthogonal polarization directions with THz spectroscopy and noticed a difference between the spectra. The hair samples are designed as a metal grid on the ring (see Figure 1.4). They observe the difference in transmittance spectra between two hair directions. The hair spectrum parallel to the THz field shows lower transmittance than the one perpendicular to the THz field, and the arranged hair works as a polarization grid. In addition, each sample is small enough to consider the results to have good accuracy. However, a significant result is that they observed the same result even in a single hair sample (Hiromoto, Shiba, & Yamamoto, 2013).

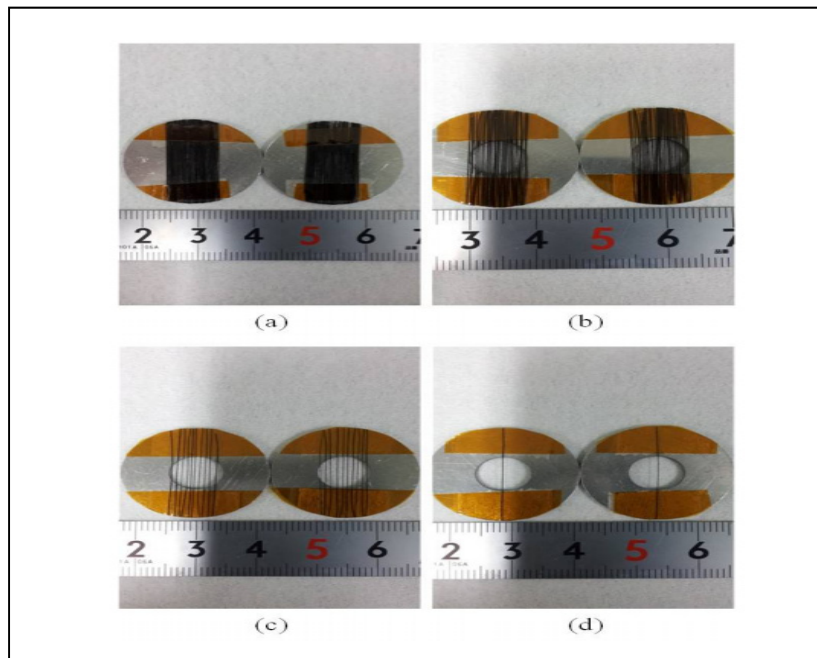


Figure 1.4 Photos of each sample, (a)80, (b)40, (c)10, and (d)1 hair. taken from Hiromoto, Shiba et al (2013)

The identification of food product adulteration is an essential process in food quality control. This adulteration is often done to blend cheap inedible ingredients for profit. Consumption of these adulterated foods can lead to serious health problems such as anemia, hypertension, and kidney failure. Detecting these adulterants in various food ingredients is a challenge for food processors. The analytical method should show fast response, easy to handle, non-destructive, and accurate. Identification of adulterants using conventional methods is time-consuming and inaccurate. Nevertheless, spectroscopic methods can provide a rapid solution for the identification of adulterants (Afsah-Hejri et al., 2019). For example, turmeric is a regular ingredient in food and even plays an important role in medicine. Yellow chalk powder is a cheap material used as a common adulterant in turmeric and can cause disease in humans. Figure 1.5 shows the change in the intensity of absorption peaks with the concentration of the adulterant (yellow chalk powder). An increase in the concentration of yellow chalk powder leads to an increase in the absorption values. The absorption values at the peaks can quantify

the amount of yellow chalk powder mixed with turmeric (Nallappan, Dash, Ray, & Pesala, 2013).

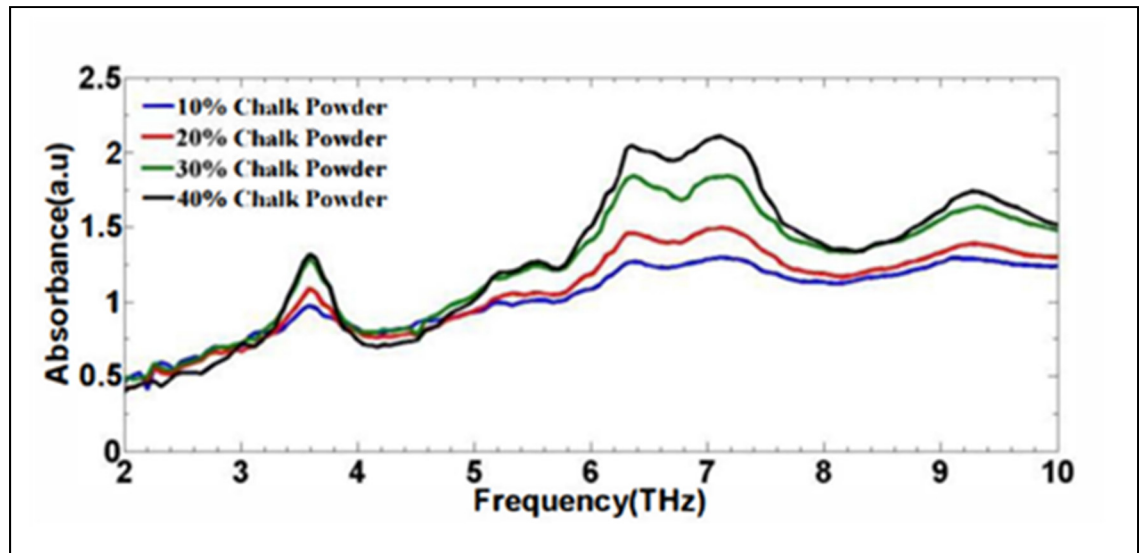


Figure 1.5 Terahertz spectrum of turmeric mixed with different concentrations of chalk powder. Taken from Nallappan et al (2013)

The consumption of melamine-tainted foods is another concern regarding the quality and safety of food products. Melamine is a nitrogen-rich molecule with an atomic number of 40 percent. Because of its high nitrogen content, this chemical is illegally added to foods such as milk powder to increase the total nitrogen concentration, which is used as an indicator to assess protein content. Melamine ingestion by pets, livestock and infants is known to cause serious health problems related to the reproductive system and kidneys. A group of researchers used Terahertz time-domain spectroscopy to study melamine in powdered milk, flour, and a chocolate bar. Different absorption peaks of melamine at 2, 2.26, and 2.6 THz were observed in all food mixtures (Baek et al., 2014).

THz spectroscopy is applicable to the identification of the THz fingerprint of antibiotics. Tetracyclines (TC) are antibiotics widely used in dairy and meat products. The overuse of this antibiotic affects human health, including toxic and allergenic reactions. For the first time, Terahertz time-domain spectroscopy was applied to detect Tetracycline Hydrochloride (TCH) in infant formula milk. All types of TCH showed clear spectra in the range between 0.3-1.8 THz. They observed an increase in absorbance as the concentration of the antibiotic increased.

Metal detectors, optical detectors, and X-ray inspection systems are widely used to investigate BFs because they are fast, economical, and reliable methods (Edwards, 2004).

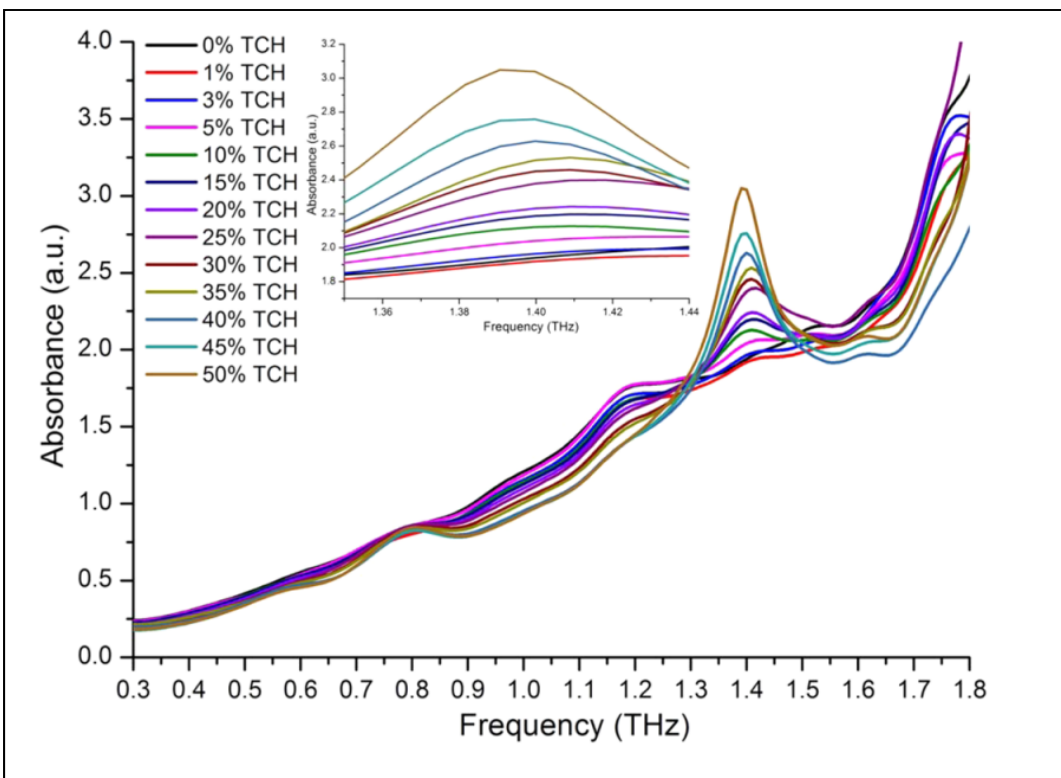


Figure 1.6 Absorbance spectra containing different kinds of TCH in infant milk powder taken from Qin et al (2014) with a zoom view in the inset

1.4 Food industry challenges

The majority of customer complaints about food safety are related to the presence of Foreign Bodies (FBs) in food. As a result, the food industry spends significant amounts of money on quality inspection equipment to maintain high product quality. Unfortunately, although many researchers and engineers have developed the technology and procedures to detect the presence of foreign objects, foreign object incidents still occur. Various techniques have been attempted and commercially developed to detect and identify FBs during the manufacturing and packaging of food products (Edwards, Stringer, & The Breakdowns in Food Safety Group, 2007). Metal detectors, optical detectors, and X-ray inspection systems are widely used to investigate FBs because they are fast, economical, and reliable methods (Edwards, 2004).

However, metal detectors can only identify metal objects. Optical detectors cannot detect internal FBs embedded in food products (e.g., glass particles in chocolate). Furthermore, although conventional X-ray systems are useful for detecting "dense" FBs (metallic and nonmetallic materials) when embedded in food products, identifying "nondense" FBs (often organic materials) is a challenge (Nielsen, Lauridsen, Christensen, & Feidenhans'l, 2013).

One of these FBs is microplastics (1 nm to < 5 mm), which are of increasing concern due to their potential effects on human and animals health (Sarker et al. 2020). Due to the universal application of plastics, microplastics are found everywhere in the environment, including soil, water, and air (Álvarez-Lopezello et al. 2020; Chen et al. 2020; Wang et al. 2021c). For example, microplastics are found in water bottles (Zhou et al. 2021) and plastic takeout containers (Du et al. 2020). In addition, researchers have found that microplastics can serve as vectors for many other contaminants such as heavy metals and antibiotics (Zhou et al. 2019; Purwiyanto et al. 2020; Yu et al. 2020b). Studies explain that the absorption capacity of heavy metals increases as microplastics age (Lang et al. 2020). Therefore, the risks of microplastics to the environment, food safety, and human and animal health could be significantly increased.

However, research on microplastics is still in its infancy, and additional efforts are needed to discover the world of microplastics. For example, there are no standard methods for extracting, identifying, and quantifying microplastics, so the results obtained by different methods may be different and incomparable (Kumar, Zhou, Tucker, & Levine, 2020). Furthermore, the multiplicity of sizes, shapes, sources, and types of microplastics makes the characterization of microplastics difficult and time-consuming (Wu et al., 2020). Therefore, it is crucial to develop new techniques for the rapid and efficient detection of microplastics (Li et al. 2020c).

Thus, unlike X-rays, which exhibit ionizing characteristics, sub-terahertz waves (millimeter waves, 30-300 GHz) and terahertz waves (0.1-10 THz) of low photon energy are non-ionizing and therefore safe, making them more suitable for use in food products. Furthermore, it is well known that radiation in these frequency ranges can detect non-dense FBs (e.g., insects and plastics) hidden in foods (Jördens and Koch, 2008, Lee et al., 2012, Ok et al., 2013). Indeed, some foods containing dry, non-polar ingredients are transparent in the sub-terahertz and terahertz wave ranges and are opaque in the visible and infrared ranges (Karpowicz et al., 2005).

1.5 Printed Electronic (PE)

PE presents an excellent combination of a wide and continuous processing area to fabricate a low-cost custom electronic device on flexible substrates using high-throughput printing methods. Printing is an environmentally friendly process, which has received enormous attention due to the reduction of material waste (Feng, Su, Happonen, Liu, & Leach, 2018). PE promises vast markets for many industries, from consumer goods, electronics, aerospace, automotive, pharmaceutical, biomedical, textile and fashion (Z. Cui, 2019). This technology has infinite potential for manufacturing packaging, sensors, and other devices that can be integrated into the design of products and objects around us (Feng et al., 2018; S. Khan, Lorenzelli, & Dahiya, 2014; Zhuldybina et al., 2019).

The history of PE began in 1977 by A. Heeger, A. G. MacDiarmid, and H. Shirakawa (Shirakawa, Louis, MacDiarmid, Chiang, & Heeger, 1977), who discovered that polymers

could be conductive by doping specific molecules. This discovery earned them the Nobel Prize in Chemistry in 2000. Following this discovery, organic semiconductors (Ebisawa, Kurokawa, & Nara, 1983) and organic photovoltaic materials (C. W. Tang, 1986) were developed in the 1980s, which is the starting point for organic electronics as a field of scientific interest. In 1991, the first organic field effect transistor was fabricated on a plastic substrate by Francis Garnier's group (Garnier, Peng, Horowitz, & Fichou, 1991). This work proved that transistors could be fabricated on plastic substrates and opened the era of plastic electronics. For example, in 1997, a fully printed transistor was made using a screen-printing technique on polyester film by Dr. Zhenan Bao (Bao, Feng, Dodabalapur, Raju, & Lovinger, 1997). Nevertheless, the recent growth in electronics is only began in 2011 when researchers, created a flexible solar cell by inkjet printing on paper (Barr et al., 2011). Following this discovery, the PE market grew rapidly and saw many developments in the printing method, leading to a large number of new applications such as (list applications here) (Watch, Watch, Data, & Computing, 2021) (see Figure 1.7)

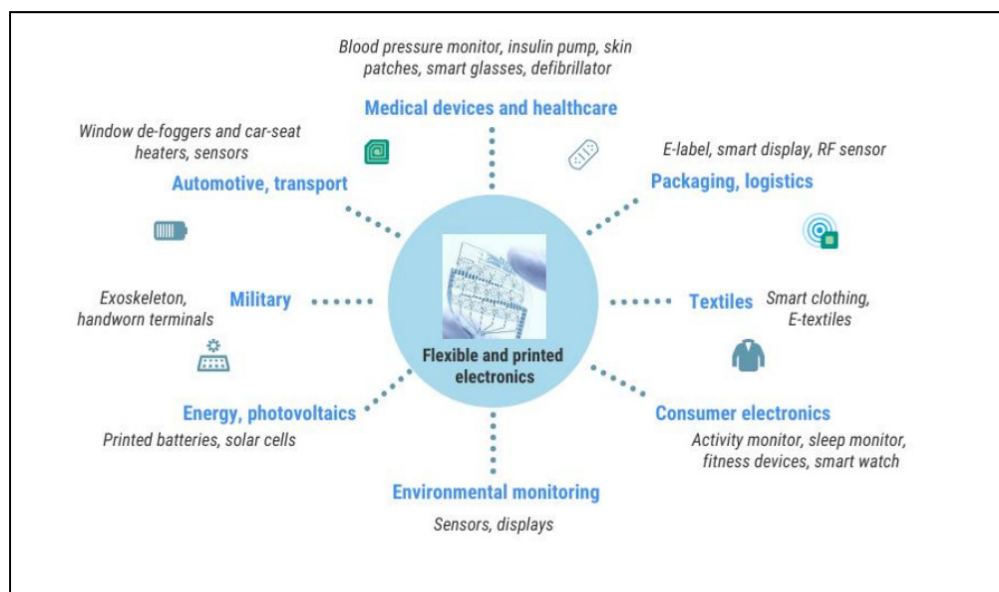


Figure 1.7 Application areas of flexible and printed electronics take from Watch, watch, Data & Computing (2021)

PE has tremendous cost and throughput advantages over lithographic fabrication processes for conventional inorganic semiconductor devices. However, PE components do not have the same high performance and reliability and will not completely replace traditional silicon-based components in the near future (S. Khan et al., 2014). The comparison between conventional manufacturing and printed electronics is summarized in Table 1.1 (Y. Khan et al., 2020)

Table 1.1 Comparison of traditional vs printable electronics taken from Y. Khan et al., [2020]

Traditional Electronics	Printable Electronics
High production cost	Low production cost
Subtractive manufacturing process	Additive process
Clean room conditions	Ambient conditions
Sophisticated fabrication (6+ steps)	Simple fabrication (3 steps)
Rigid substrates	Any kind of substrates
Small area	Large area
High integration density	Low integration density
Short switching times	Long switching times
High resolution	Low resolution
Constant repeatability	Low repeatability
Long product lifetime (~10 years)	Short product lifetime (~ 0.1 year)
Established fabrication method	Early-stage technology

1.5.1 Printable electronic material

Printable electronic material contains two different part Function ink and substrate which in the following subsections are described in detail.

1.5.1.1 Functional ink

PE components require specific ink functionalities. Nowadays, several types of conductive, semiconductive, and dielectric inks are commercially available (Ko et al., 2007). Conventional ink is formulated from functional materials, vehicles, resins and additives. The resins have the most significant influence on the properties of the ink and determine the bonding of the formulation ingredients to each other and the adhesion with the substrate. The liquid part of the formulation is a vehicle for transferring the ink into the substrate and setting the drying rate. Additives improve the functional material properties or provide additional properties (Kamyshny & Magdassi, 2014). Ink development is in high demand, mainly with the transformation of existing electronics to eco-friendly, bio-based, and biodegradable PE to lighten the environmental footprint of electronics (Mirka et al., 2019).

1.5.1.2 Substrate

Some PE printing techniques are capable of using traditional, inflexible substrates such as silicon or glass (Keskinen, 2012). In this case, PE techniques can be directly compared to traditional production techniques such as those used in printed circuit board manufacturing. However, one of the main advantages of PE methods is the ability to use flexible substrates. Compared to traditional methods, the processing temperature of the entire process is compatible with the use of low-cost plastic films. which are generally non-porous and can withstand all manufacturing steps, including pre- and post-printing processes (Trudeau et al.,

2017). Frequently used substrates are Polyimide (PI), Polyethylene Terephthalate (PET), or Polyethylene Naphthalene (PEN) sheets (Keskinen, 2012) .

1.6 Existing printing methods

Flexographic printing is a high-speed continuous R2R process, a well-known manufacturing method generally used by the packaging industry (Rossander, Zawacka, Dam, Krebs, & Andreasen, 2014). Figure 1.8 shows the basic system of flexographic printing. First, ink is brought into contact with a micro-engraved cylinder (anilox) and fills its cells, which is then scraped with a doctor blade to ensure that the cells are filled with a controlled and consistent volume of ink (Bould, Claypole, & Bohan, 2004; Kipphan, 2001).

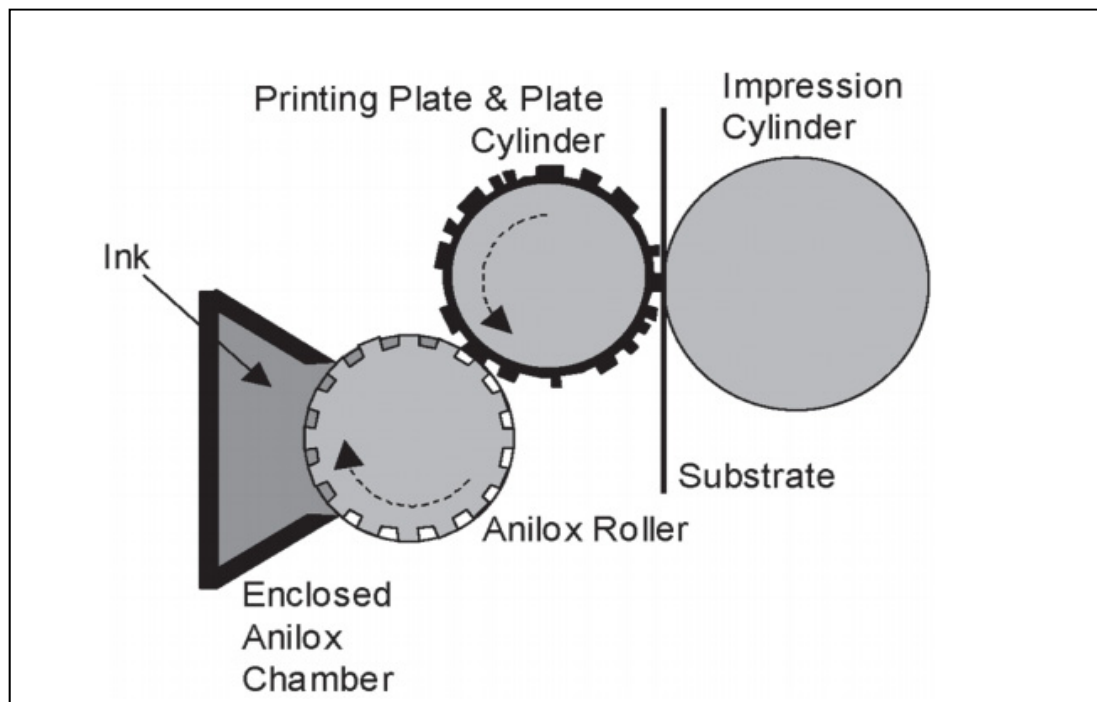


Figure 1.8 A schematic diagram of flexography printing taken from Clapole & Bohan (2004)

Then the inked design is pressed against the substrate in the nip between the printing form and a printing cylinder. The ink is transferred to the substrate with the lowest pressure. Because of the low pressure used in the nip, flexography can transfer ink to a wide variety of substrates, ranging from fragile substrates such as corrugated cardboard that could be crushed during printing and self-adhesive labels that contain a layer of adhesive to smooth substrates such as plastics, foils or glass. The thickness of the printed film is defined by the anilox parameters and the transfer rates from the plate cylinder to the printing substrate (Kipphan, 2001).

1.7 THz waves and printed electronics

As mentioned before, the terahertz (THz) bands (0.1–10 THz) have demonstrated growing applicability to communications, materials, medical, chemical, and life sciences over the past two decades (J. Federici & Moeller, 2010; McIntosh et al., 2012). To manipulate these waves in a simple and cost-effective manner, an emerging manufacturing process appears to be a key solution to produce these types of needed devices, namely printed electronics (PE) (Münzenrieder et al., 2020). Due to the printing resolution and relatively long wavelength of THz waves, it is now easily possible to print devices with sub-wavelength resolution in the THz frequency range without the need for a clean room (Balocco et al., 2010).

An example is the fabrication of split-ring resonator arrays (SRRs) designed for gigahertz to THz frequencies by inkjet printing. Their resonant behavior is studied by THz spectroscopy and compared to structures fabricated by conventional microfabrication techniques. Their results show that inkjet printing, which has the advantage of being a fast, flexible and low-cost alternative to conventional microfabrication techniques, can be considered as a method for the fabrication of THz metamaterials. Another study showed that THz metamaterials were successfully fabricated using Electro Hydro Dynamic (EHD) jet printing and used as sensors. In this work, two different substrates are used for metamaterial sensors: silicon and polyimide (PI). EHD jet printing was used to print tiny patterns of high-resolution metamaterial structures

on both substrates. Experimental characterization and simulation were conducted to study their performance in detecting yeast of different weights. The results showed that the metamaterial sensor fabricated on the low-index substrate (the flexible PI film) had six times the sensitivity of the metamaterial sensor fabricated on the higher-index substrate (the wafer). The thin, flexible PI film also yielded higher sensitivity due to its thin thickness, which makes its effective dielectric constant close to the dielectric constant of air. The use of a thin substrate can provide a useful guideline on how to significantly improve sensitivity in metamaterial detection (Tenggara, Park, Yudistira, Ahn, & Byun, 2017). In 2016, Farid et al. used inkjet printing technology to produce THz range metal gate polarizers (see Figure 1.10) using THz spectroscopy.

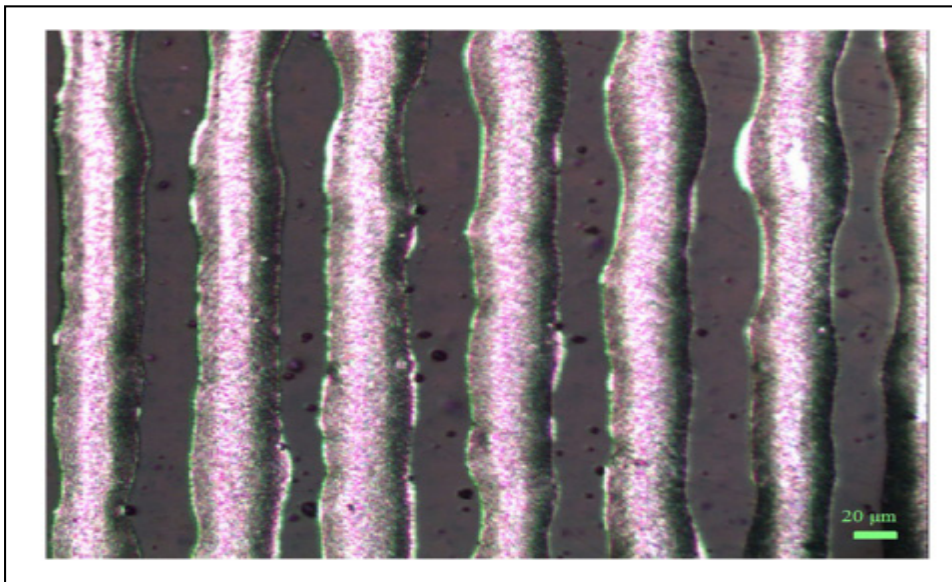


Figure 1.9 An image of the 40 μm gap, 40 μm width wire grid polarizer with four layers (40G/40W/4L)

They investigated the effect of three parameters on the ability of the polarizers, namely the spacing between the silver ink lines, the width of the ink lines and the number of passes with the inkjet printer. They also studied the effect of stacking multiple polarizers on the degree of polarization. They found that decreasing the spacing between the ink lines, decreasing the width of the ink lines, and increasing the number of layers resulted in a higher degree of

polarization within the parameters of their experiment and the method used for printing. They confirmed that these simple polarizers, when stacked, are comparable to commercial polarizers. The polarizer topology consisting of lines with a spacing of 40 μm and a width of 40 μm is very efficient in the frequency range of 0.3-1 THz. Further reduction in gap size can also increase the degree of polarization, and more stacking of these polarizers can show ultimate capability for polarization.

In terms of PE performance, obtaining uniform, continuous, and high-quality printed features is crucial to achieving the printed layers' reliable electrical and electronic properties (Seung et al., 2007). The PE quality can be evaluated using scanning electron microscopy (SEM). Nevertheless, this method is time-consuming, as it requires a vacuum environment (Cook et al., 2013). The automated imaging technique is based on digital cameras to capture 2D images of dispersed particulate samples, but it cannot provide electrical properties (Venkataraman et al., 2006). Researchers' recent work is based on THz sensing, which is introduced for monitoring the quality of inkjet-printed electronics. The results show that THz-TDS-based imaging can both map and characterize the printed electronic-inkjet samples (see Figure 1.9) (Zeng et al., 2017).

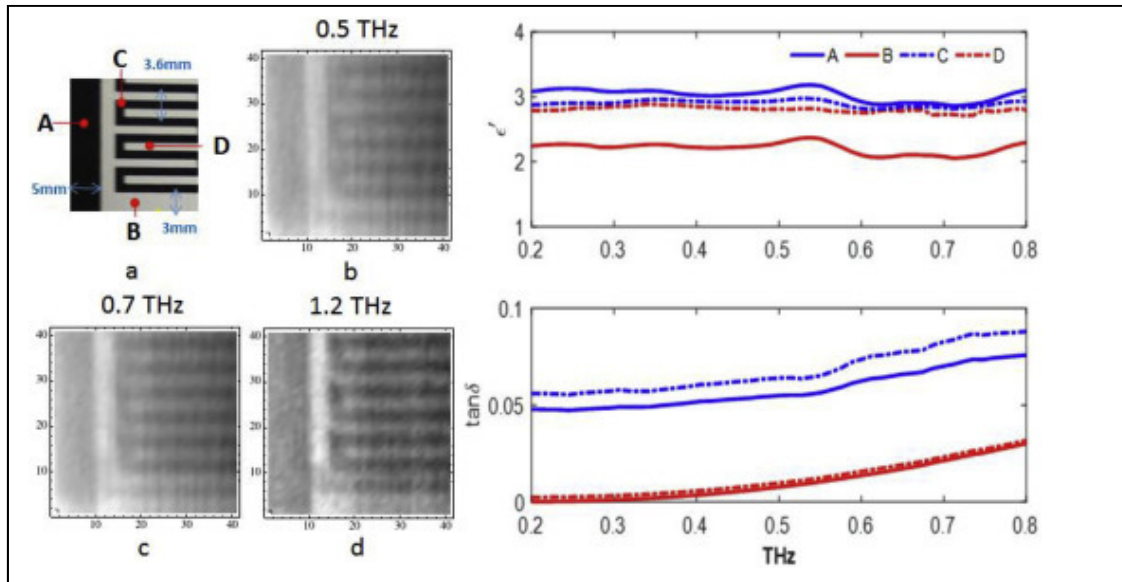


Figure 1.10 Transmission imaging measurement of a printed meander-line pattern by THz-TDS. Left: images at selected frequencies; Right: permittivities and loss tangents at selected points

Finally, it is worth mentioning that our group has recently acquired an important expertise in the non-destructive testing of PE production through a quality control bar made of a specially designed metasurface. This new approach clearly demonstrates the timely relationship between PE manufacturing and THz wave capabilities (Zhuldybina, Ropagnol, & Blanchard, 2021; Zhuldybina et al., 2020; Zhuldybina et al., 2019)

CHAPTER 2

METHODOLOGY

2.1 Introduction

This chapter describes THz Time-Domain spectroscopy and its techniques. It then explains the reflection and transmission modes. After it describes how THz waves are generated and detected by a photoconductive antenna. Finally, it defines the setup and sample preparation for this study.

2.2 THz Time -Domain Spectroscopy (THz-TDS)

The study of the energy, wavelength, or frequency of photons passing through a sample of matter is called spectroscopy. Since the 1950s, spectroscopy in the far-infrared field has become achievable with the development of FTIR spectroscopy (Loewenstein (1966); Möller & Rothschild (1971)). The FTIR technique records data by the path difference (also known as time difference) domain. This method provides fast data acquisition, improves the signal-to-noise ratio, and limits the detector noise level to the source noise level (Fellgett (1949)). However, the low-energy photons of FTIR sources, the low resolution in the FIR region, and the absence of appropriate optical elements (e.g., Beam Splitter(BS)) are disadvantages of this method ((Storm et al., 2012). In addition, this method cannot directly characterize a material because it only provides the light transmission intensity without information on the phase parameters (Dexheimer, 2007).

In the late 1980s, femto-second (fs) lasers provided an alternative method of spectroscopy in the THz region, opening a new door to materials characterization. Similarly, the mode-locked fs laser introduced in the 1990s considerably improved the use of time-domain spectroscopy studies on various materials (Zhang & Yan, 2001). Based on the optical excitation of photoconductive dipole antennas, this method is known as THz-TDS (Van Exter, Fattinger,

& Grischkowsky, 1989). It is closely related to Ti: fs sapphire laser (Titanium femtosecond laser) technologies (J. Hilton, P. Prasankumar, A. Trugman, J. Taylor, & D. Averitt, 2006).

2.2.1 THz-TDS system

To perform THz-TDS, a typical spectrometer consists of an ultrashort pulse laser, a delay line, a THz transmitter, a THz detector, and a set of optical components to operate the radiation with the system. Figure 2.1 shows an illustration of a time domain spectrometer.

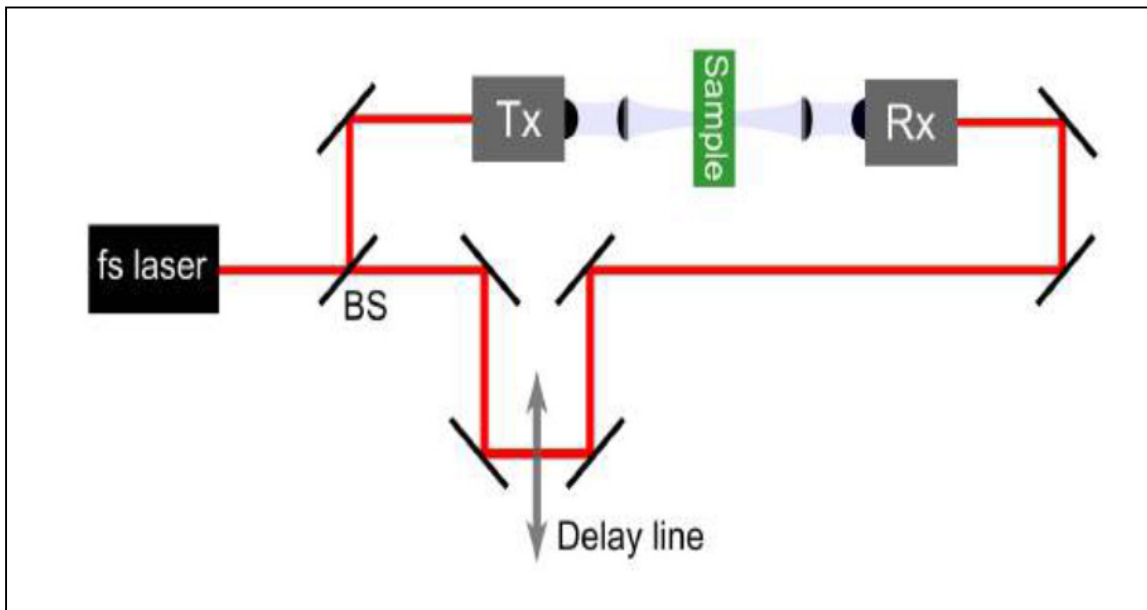


Figure 2.1 Diagram of a THz TDS spectrometer in transmission geometry. A beam splitter divides the ultrashort pulse. A mirror guides one part to the transmitter for terahertz generation, and the other part is guided by a set of mirrors through the delay line and then to the receiver for terahertz detection

The near-infrared laser provides ultrashort pulses; each radiation cycle is split into two optical pulses by a beam splitter. One of the pulses is sent to the THz emitter, and the generated THz radiation is collected, collimated, and focused on a sample by a pair of lenses (in the free space). The second pair of lenses collects the radiation after interaction with the sample and

refocuses it on the detector. The beam path of the second optical pulse is modified by a delay line to detect the THz radiation from the sample. The emission and detection processes are described in more detail in the following paragraph.

2.2.2 Emission and detection of terahertz radiation

In the early 1990s, the use of THz spectroscopy has expanded rapidly in science and technology for a wide variety of uses. Since the early pioneering work of Grischkowsky and colleagues, a number of materials and emission and detection techniques have been studied. In general, there are two main ways to generate and detect pulsed THz radiation from femtosecond laser pulses: the Photo Conductive Antenna (PCA) and nonlinear optical materials. THz spectroscopy uses two types of photoconductive antennas: a polarized PCA to generate THz pulses and a non-polarized PCA for detection. There are many reasons to use PCA for THz spectroscopy and imaging.

- Operates at room temperature and does not need cooling.
- Is small in size
- Does not require high-voltage power sources;

2.2.2.1 Terahertz generation by PCA

PCA is a fundamental technique for generating THz radiation. The unique structure of the PCA is embedded in a semiconductor, such as a low-temperature Gallium Arsenide (GaAs) substrate, consisting of two metal electrodes with a small gap like a radio dipole, typically with 5- μm gap size that supports a large electric field across its surface.

For the PCA emitter, the "pumping" pulses of the femtosecond lasers (800 nm at 1.5eV), is focused on the gap between the two electrodes and propagates into the semiconductor. Since the photon energy propagated into a semiconductor is slightly higher than the bandgap, photons are absorbed by the substrate. Consequently, electron-hole pairs are created inside the

conduction band of the semiconductor crystal. Excited photocarriers are accelerated on a subpicosecond time scale. This rapid rise and fall of the transient photocurrent is the source of a THz electromagnetic field irradiated away from the antenna. (Guerboukha et al., 2018) The electric field of the THz radiation E_{THz} is proportional to the time derivative of the photocurrent, defined as:

$$E_{THz(t)} \propto \frac{dj}{dt} \quad (2.1)$$

Where dj is bias field.

The energy of the THz pulse is mainly extracted from the voltage source rather than the optical source. This allows to PCA emitters to be particularly efficient even when pumped with low intensity such as the one from an oscillator Ti: Sapphire laser. Of course, this is the main advantage of PCA in comparison with nonlinear crystal for optical rectification. Unfortunately, increasing the bias voltage can induce thermal avalanche effect which can lead to the destruction of the PCA. The THz waves generated by the PCA diverge significantly, which might be a concern when collecting THz waves in free space. In general, commercial PCAs feature a hemispherical high resistivity silicon lens connected to the back of the substrate. This connection reduces the number of THz pulse reflections that can occur because of an air gap. Furthermore, at THz frequencies, silicon ($n = 3.47$) has an excellent refractive index match with GaAs ($n = 3.6$), reducing reflection losses. At THz frequencies, silicon exhibits low dispersion and absorption. Finally, the THz pulses propagate to the detectors through in the THz lenses and are collected and focused by a silicon lens located on the THz detector. The emission process is represented graphically in figure 2.2.

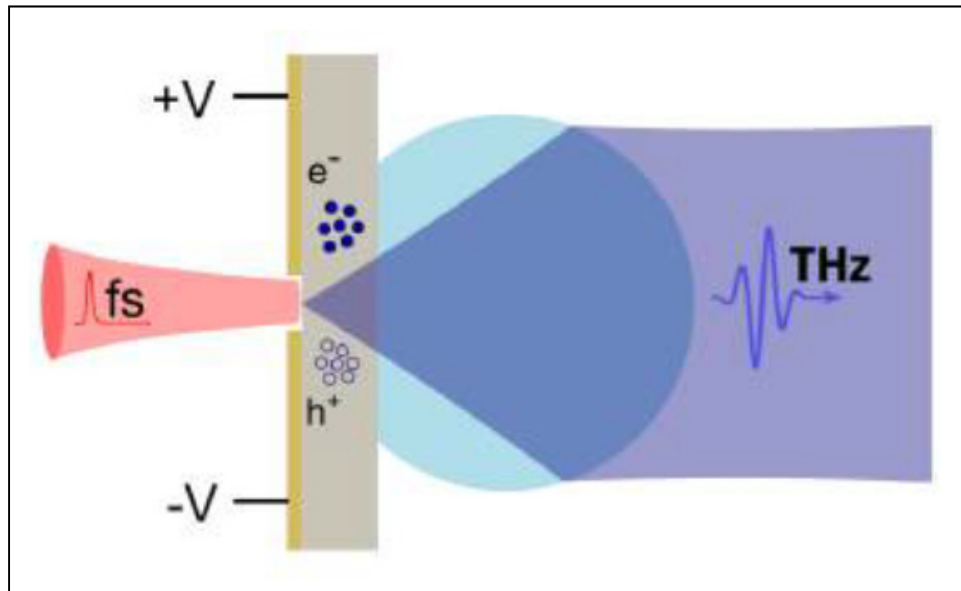


Figure 2.2 Terahertz generation by a photoconductive antenna

2.2.2.2 Terahertz detection

THz detection can be achieved with a PCA similar to THz generation. However, there is no external polarization for the metal space fabricated on the semiconductor,(Pradarutti et al., 2008) as shown in Figure 2.3. The electric field of the THz pulse creates an electric polarization. A laser beam focused on a semiconductor gap creates free carriers that increase the conductivity of the PCA. Thus, a current is generated which is proportional to the THz electric field. The duration of the laser pulse and the lifetime of the carriers, affect the response function of the detector. In contrast to the generation situation, where the input power also affects the length of the current pulse, here only the carrier lifetime is critical for the detection. Short carrier lifetimes produce high temporal responses, resulting in larger THz bandwidths. In LT-GaAs, carrier lifetimes are typically between 100 and 300 fs. The THz induced current ranges from picoamperes to nanoamperes.

The photocurrent between the electrodes would be proportional to the integral of the electric field for each value of the relative delay given by

$$J(t) = \int_{-\infty}^{+\infty} E_{THZ}(t') \sigma(t - t') dt' \quad (2.2)$$

Where $J(t)$ is the photocurrent, E_{THZ} is the THz electric field, t is the relative delay between pulses, and σ is the conductivity of the antenna induced by the ultrashort pulse (Jepsen, Jacobsen, & Keiding, 1996). A graphical representation of the terahertz detection process can be seen in Figure 2.3.

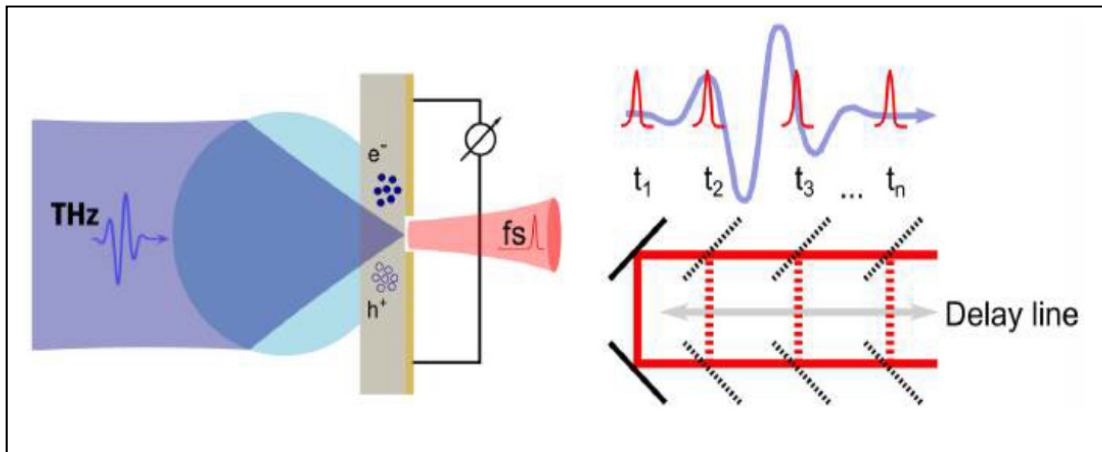


Figure 2.3 Terahertz detection by a photoconductive antenna

2.3 THz-TDS technique

In order to perform spectroscopic studies with the THz-TDS technique, an electric field is recorded as a function of time using a time domain system. Then, the recorded information is processed to retrieve the THz characteristics of the studied material. Terahertz time domain systems can be configured in transmission or reflection mode (Baxter & Guglietta, 2011).

2.3.1 Transmission mode

Transmission can be defined as a method where THz radiation is transmitted through matter. THz radiation strikes a medium and is transmitted through it, and is affected as follows:

1. Its intensity reduces as the THz radiation penetrates deeper inside the medium due to absorption and scattering.
2. Its velocity becomes lower in the medium than in the air (Shan, Nahata, & Heinz, 2002).

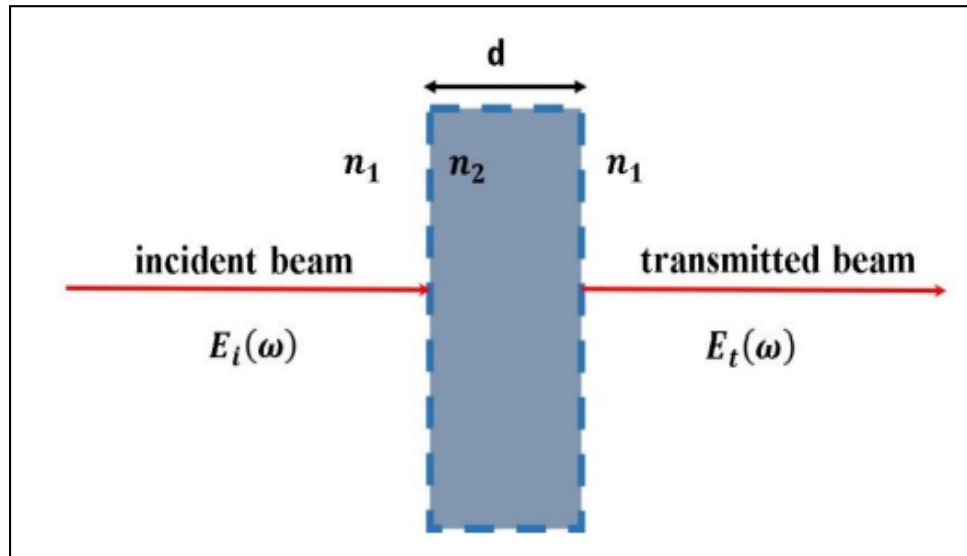


Figure 2.4 Geometry for Electric Field Transmission of incident waves with amplitude E through a layer of thickness d with refractive index n_2

Figure 2.4 shows the transmission model, which explains how a radiation beam propagates through the medium. In transmission mode, incident radiation (E_i) with frequency and complex refractive index n_1 passes through a medium with thickness d and complex refractive

index n_2 . The complex transmission, as a function of the frequency ω of the THz pulse in medium one and medium two after transmission, can be expressed as:

$$E_{ref} = E_i(\omega) = E_0(\omega)e^{i(\omega t - k_1(\omega)x)} \quad (2.3)$$

$$E_{sam} = E_t(\omega) = E_2(\omega)e^{i(\omega t - k_2(\omega)x)} \quad (2.4)$$

Where E_0 and E_2 are the electric fields of the THz pulse in the air (medium 1) and sample (medium 2), respectively. k_1 and k_2 represent the wavenumbers in the air (medium 1) and sample (medium 2), respectively. x is the optical path, which is equal to sample thickness (Swift, 2008).

The complex transmission for normal incidence is defined using equations (2.3) and (2.4), taking the ratio of the transmission of the sample ($E_{sam}(\omega)$) and reference ($E_{ref}(\omega)$) as;

$$T(\omega) = \frac{E_{sam}(\omega)}{E_{ref}(\omega)} \quad (2.5)$$

To calculate the refractive index and absorption coefficient, the complex refractive index of the sample is given as;

$$\tilde{n}(\omega) = n(\omega) - ik(\omega) \quad (2.6)$$

Where $n(\omega)$ and $k(\omega)$ are the real and imaginary parts of the sample complex refractive index, $\tilde{n}(\omega)$, respectively. The extinction coefficient is determined by:

$$K(\omega) = \frac{\alpha(\omega)c}{2\omega} \quad (2.7)$$

Where α represents the absorption coefficient.

In the case of a normal incident, where the THz pulse is directly transmitted into the medium, the Fresnel transmission coefficients, T_{12} and T_{21} , are defined at each face: $T_{12} = 2n_1 / (n_2 + n_1)$ and $T_{21} = 2n_2 / (n_1 + n_2)$. Finally, the real part of the refractive index $n(\omega)$ and absorption coefficient $\alpha(\omega)$ of the sample is determined from equations (2.3), (2.4), and (2.5);

$$n(\omega) = 1 + \frac{c}{\omega d} (\varphi_{sam} - \varphi_{ref}) \quad (2.8)$$

$$\alpha(\omega) = -\frac{2}{d} \left(\frac{(n(\omega)+1)^2 E_{sam}}{4n E_{ref}} \right) \quad (2.9)$$

Where φ_{sam} and φ_{ref} describe the accumulative phase of the THz pulse propagated along the optical path, determined by the complex exponentials $e^{i(\omega t - k_2(\omega)x)}$ and $e^{-i(\omega t - k_1(\omega)x)}$ of the sample and reference, respectively.

2.3.2 Reflection mode

The reflection mode is the second measurement model. It is difficult to measure the optical characteristics of many materials, such as biological tissues, in transmission mode because their absorption is too high to transmit THz radiation. Thus, the reflection mode is used to measure these materials. Figure 2.5 shows the reflectance signal measurement in reflection mode.

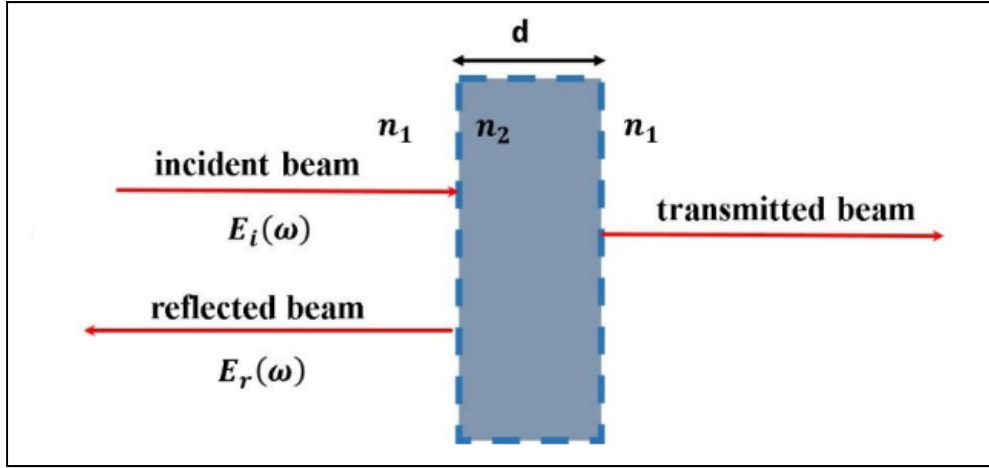


Figure 2.5 Reflection geometry for complex-response measurement in a sample with thickness d

THz pulses are focused on the surface layer of a sample with thickness d , electric field E_i , and refractive index n_1 . The THz pulse E_r is reflected at the air/sample interface, where the refractive index changes from low to high. Hence the reflection amplitude $R(\omega)$, defined by the ratio between the sample spectrum and the reference spectrum, (Guerboukha et al., 2018)

$$R(\omega) = \frac{E_{sam}(\omega)}{E_{ref}(\omega)} \quad (2.10)$$

Which is 2.10 equation is equal to:

$$R(\omega) = \frac{t_{12}r_{23}t_{21}}{r_{12}} \exp\left(-\frac{in_2\omega L}{c}\right) = \frac{4n_1n_2}{n_1^2-n_2^2} \exp\left(-\frac{in_2\omega L}{c}\right) \frac{n_2-n_3}{n_2+n_3} \quad (2.11)$$

If we assume that media 1 is air ($n_1 = 1$) and media 2 is a window of a known refractive index ($n_2=n_w$), Eq. (2.11) can be written as:

$$c = \frac{E_{sam}(\omega)}{E_{ref}(\omega)} \frac{1-n_w^2}{4n_w} \exp\left(\frac{in_w\omega L}{c}\right) = \frac{n_w-n_3}{n_w+n_3} \quad (2.12)$$

Then, $n_3(\omega)$ can be found analytically as:

$$n_3(\omega) = \left[\frac{1-c}{1+c} \right] n_w(\omega). \quad (2.13)$$

2.4 Experimental setup for printed polarizer

To analyze the quality of a printed polarizers, we used a conventional THz-TDS with two PCA as an emitter and detector in transmission mode. The laser excitation parameters of the PCAs emitter and detector are the same as for the experiment for the dog food. The PCAs were pumped using a Ti: Sapphire laser oscillator providing 810 nm, 40 fs laser pulses at a repetition rate of 80 MHz and an average power of 20 mW on each antenna. The emitter generates a vertically polarized THz beam. The detector receives the THz pulse, which has passed through the sample (see Figure 2.6).

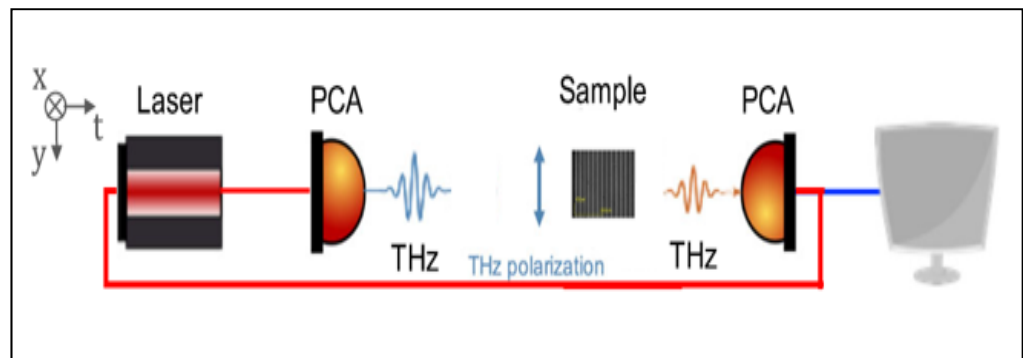


Figure 2.6 Terahertz Time-Domain setup

2.5 Sample preparation

The polarizer is designed with the identical 50 μm -line widths, spacing, and unit cell. WGsPs have been produced using an industrial roll-to-roll press with the flexography printed unit. The silver ink (NovaCentrix PFI600) has been printed onto the PET substrate (125 μm -thick) at the production speed of 15 m/min. The printed devices have been dried in line with the hot air at the temperature of 100 $^{\circ}\text{C}$. The conductivity of 4.4×10^6 S/m was obtained using four-point probes. The thickness of 352 nm was evaluated using Contour GT-K Manual Optical Profilometer, Bruker. Figure 2.7 shows the image of printed polarizers taken with a LEXT 4100 optical microscope.

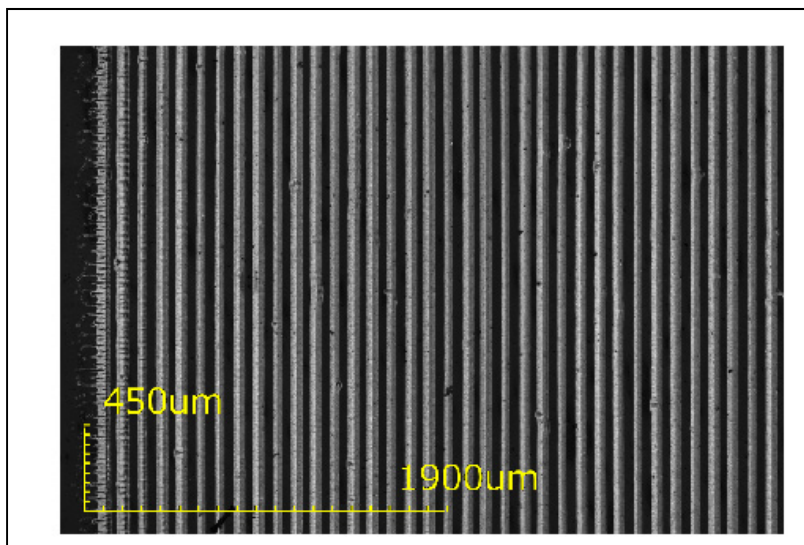


Figure 2.7 A visible image of a printed polarizer

2.6 Experimental setup for powder spectroscopy

We applied a THz-TDS system based on the transmission and detection of THz waves by two PCAs from TeraVil Ltd. The PCAs were pumped using a Ti: Sapphire laser oscillator providing 810 nm, 40 fs laser pulses at a repetition rate of 80 MHz and an average power of 20 mW on each antenna (see Figure 2.8a).

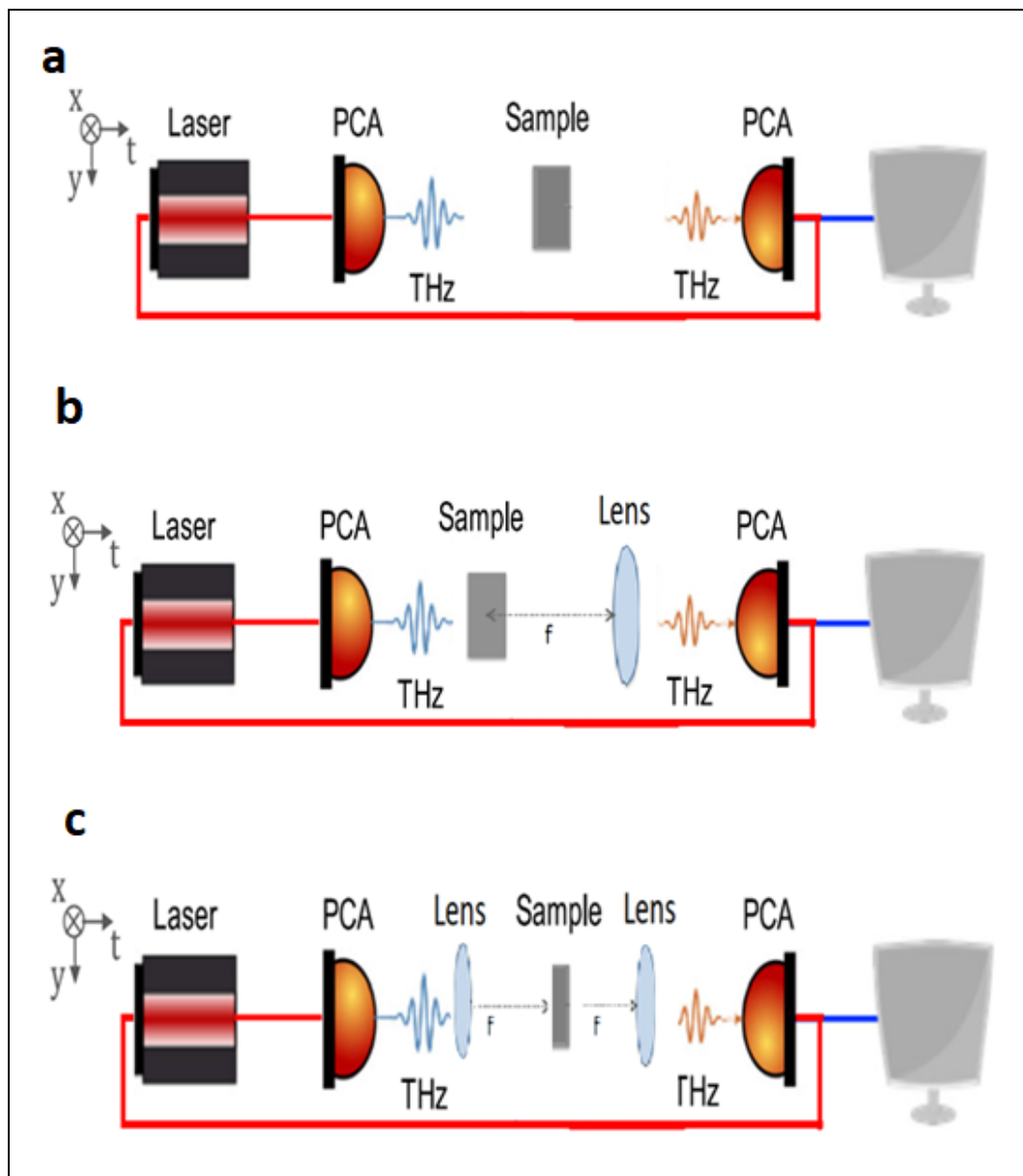


Figure 2.8 a; THz-TDS system ,b; THz-TDS system with one lens, c;
THz-TDS system with two lenses

After not getting the right result with the first configuration, we designed two other configurations. The first hypothesis is that the powder will create the dispersion of the THz wave, which requires a lens to collect the signal correctly at the detection position. Thus, the Teflon lens, right after the sample, collimates the THz output beam with a diameter of about 10 mm. As shown in Figure 2.8b, the collimated THz beam is collected by a PCA detector.

The second assumption is that a lens placed in front of the sample would allow for better coupling onto the sample and better signal recovery at the detection end, i.e., it would collect more photons, which would improve the detection signal. This third configuration is shown in Figure 2.8c.

We have also designed a sample holder, which holds a sample in the exact place without any tilt, i.e. having free standing powder without applying any pressure (see Figure 2.9). In order to know about dimensions of sample holder see the appendix 1.

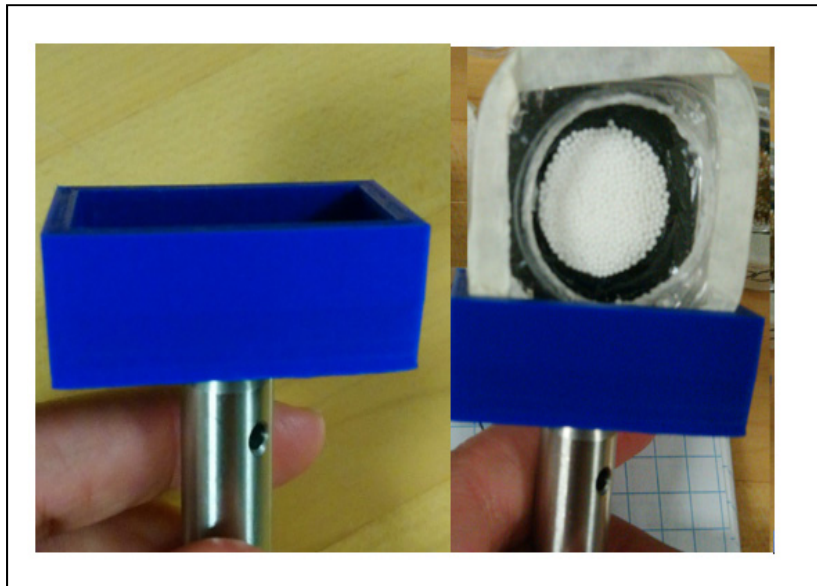


Figure 2.9 Sample holder

To demonstrate the detection of contaminant plastic in feed powder, we prepared a series of samples with a specific percentage of contaminant (plastic) per volume.

For this demonstration, we bought micrometer calibrated plastic spheres from Cospheric. The model is WPMS-1.35 850-1000 um – for a quantity of 10g. The plastic particles are completely round, and their diameter varies between 0.85 and 1.00 mm.

We prepared five samples with different percentages of plastic. First, we measured the empty sample box with a digital scale. As shown in the Figure 2.10, it is 6 g. Then, we measured only the amount of animal food that could fill the sample box but without the box, which is 0.999 g. Therefore, we can calculate the total weight of the 0% plastic sample (6g +0.999: 7 g). Similarly, we performed all these steps for a 100% plastic sample, and the total weight was the same as the 0% plastic sample.



Figure 2.10 Measurement of the empty sample box with a digital scale

In order to measure exactly 20% plastic, we calculate:

$$(20\% \times \text{Total weight of plastic}) + (80\% \times \text{Total weight of animal food}) \quad (2.14)$$

Therefore, the weight of 20% plastic sample is 0.799. The table below shows the weight of all samples.

Table 2.1 Weight of all samples

Sample	Empty Sample Box Weight(g)	Plastic Weight(g)	Animal Food Weight(g)	Total Weight Of Each Sample(g)
0% plastic	6.000	0.000	0.998	6.998
20% plastic	6.000	0.199	0.799	6.998
33% plastic	6.000	0.333	0.665	6.998
50% plastic	6.000	0.499	0.499	6.998
100% plastic	6.000	0.998	0.000	6.998

Figure 2.11 shows that the photo of each sample that we provide to our study.

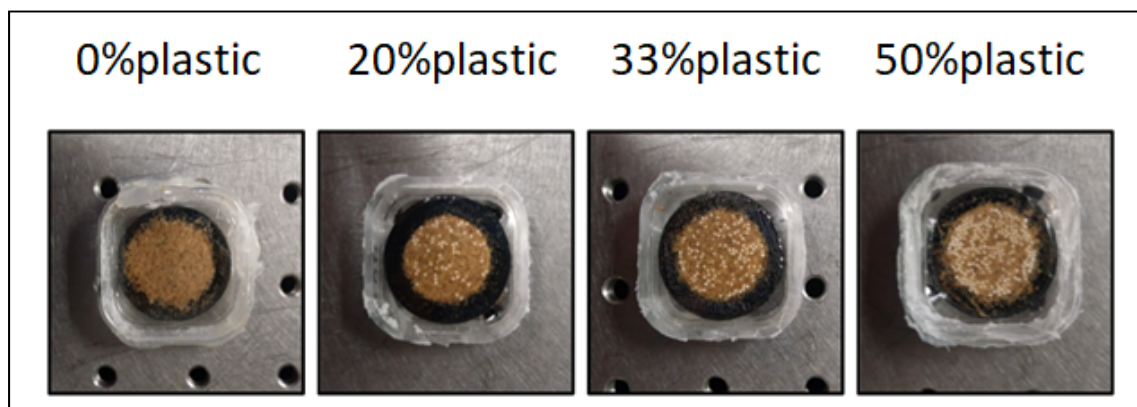


Figure 2.11 Animal food samples

2.7 Reflection spectroscopy and simulation

We applied a THz-TDS system based on the reflection and detection of THz waves by two PCAs from TeraVil Ltd. The PCAs were pumped using a Ti: Sapphire laser oscillator providing 810 nm, 40 fs laser pulses at a repetition rate of 80 MHz and an average power of 20 mW on each antenna and THz beam by means of a set of mirrors was focused on the sample and after specular reflection was collected and focused on the detector (see figure 2.12)

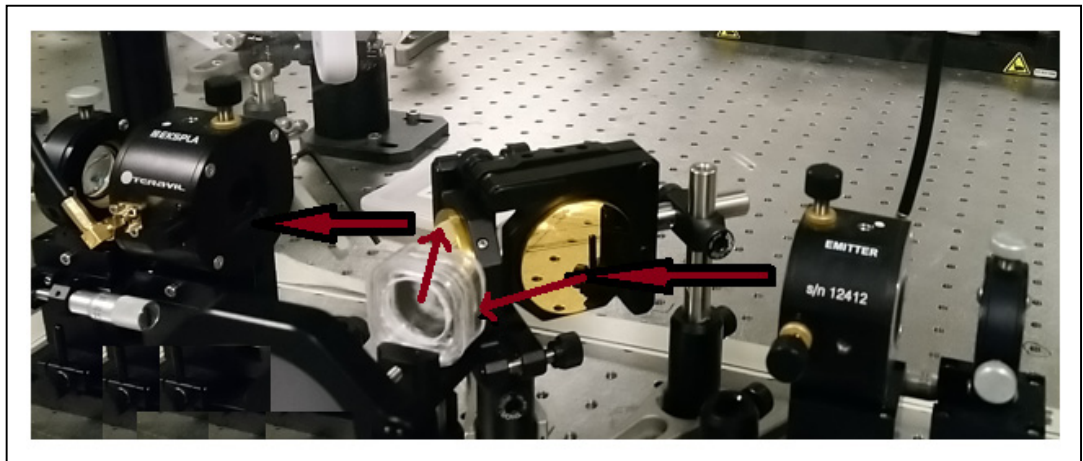


Figure 2.12 Reflection spectroscopy set-up

The samples prepared for this experiment were the same as those samples which are tested in The transmission spectroscopy, expected this time the Aluminum(Al) sheet was used as a reflector. As an example figure 2.13 shows 33% plastic sample with Al (see figure 2.13)



Figure 2.13 Sample with 33% plastic and Aluminum(Al)

The first measurements obtained in reflection being very complex, we decided to perform simulations of this experiment. Indeed, the measurements in reflection produce multiple echoes coming from the sample and the sample support. This problem greatly complicates the data analysis.

In order to simulate the effect of the particle with a similar refractive index on the THz field in a reflection mode, we used Lumerical Finite-Difference-Time-Domain (FDTD) software. In the simulation, the incoming THz beam is assumed to be Gaussian with a central frequency of 0.83 THz and a bandwidth of 2.5 THz. Finally, the incident on samples and then the reflected THz signals are recorded by a monitor.

The following Figure (2.14) is a simulation of reflection THz spectroscopy and four rectangles represent a sample. In this simulation each sample consist of four materials. One material is paly as a reflector wich here is gold (yellow rectangle) and three other materials (three blue rectangels) have different refractive index(n).

Sample 1: Comprises a reflector (gold (Au)) and three particles with a refractive index of 1.05.

Sample 2: Comprises a reflector, and three different particles with 1.05,1.1,1.05 refractive index.

Sample 3: Comprises a reflector , and has three other particles with 1.05, 1.1, 1.1 refractive index.

Sample 4: Comprises a reflector and three particles with 1.1,1.1,1.1. The distance between each sample is $100\ \mu\text{m}$. And the thickness is 1mm;

The idea behind this experiment is to see if the THz spectroscopy signal in the time domain can differentiate in time the different positions of each sample. This is a difficult task since the wavelength of 1 THz corresponds to $300\ \mu\text{m}$, which is larger than the separation between the particles (e.g. $100\ \mu\text{m}$). To assist in the temporal discrimination between these particles, we used wavelet transform analysis. Wavelet analysis is a widely used tool (Sato et al., 2006). Unlike the fast Fourier analysis, the wavelet analysis studies the variation of the frequency as a function of time . This mathematical operator displays the broadband spectra of the THz wave in its different frequency components separated as a function of time. Nevertheless, our preliminary wavelet results presented in the next section are not yet very conclusive.

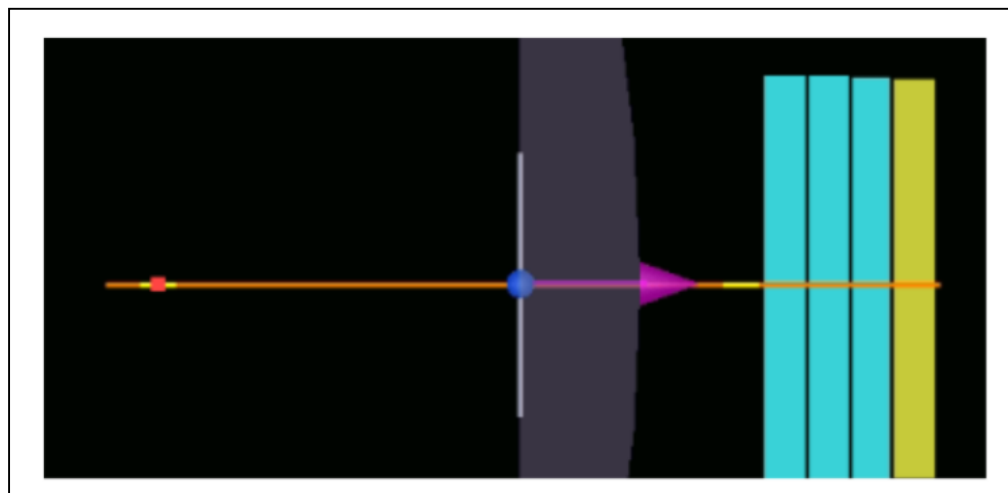


Figure 2.14 Reflection simulation with a sample

CHAPITRE 3

RESULTS AND ANALYSIS

3.1 Introduction

This chapter describes the results obtained from two research projects.

First, it explained the animal's food quality control results. After that, it described the experimental results of polarizer quality control. All results in this chapter are defined precisely by details and figures.

3.2 Animal food powder results

THz transmission data were analyzed in the time and frequency domain to identify the internal structure of the samples, detect contaminants, and differentiate samples with and without plastic particles. The granularity of the samples, due to heterogeneous, complex, uneven surfaces and tilt, affected the measurements, scans and spectra of the THz system, increasing scattering effects (Franz, Fischer, & Walther, 2008). Therefore, we tried to find solutions to avoid all these undesirable problems.

Chapter 2 (Methodology) mentions that the first transmission setup was designed without a lens (see page 45 to see the first transmission setup) and without a sample holder.

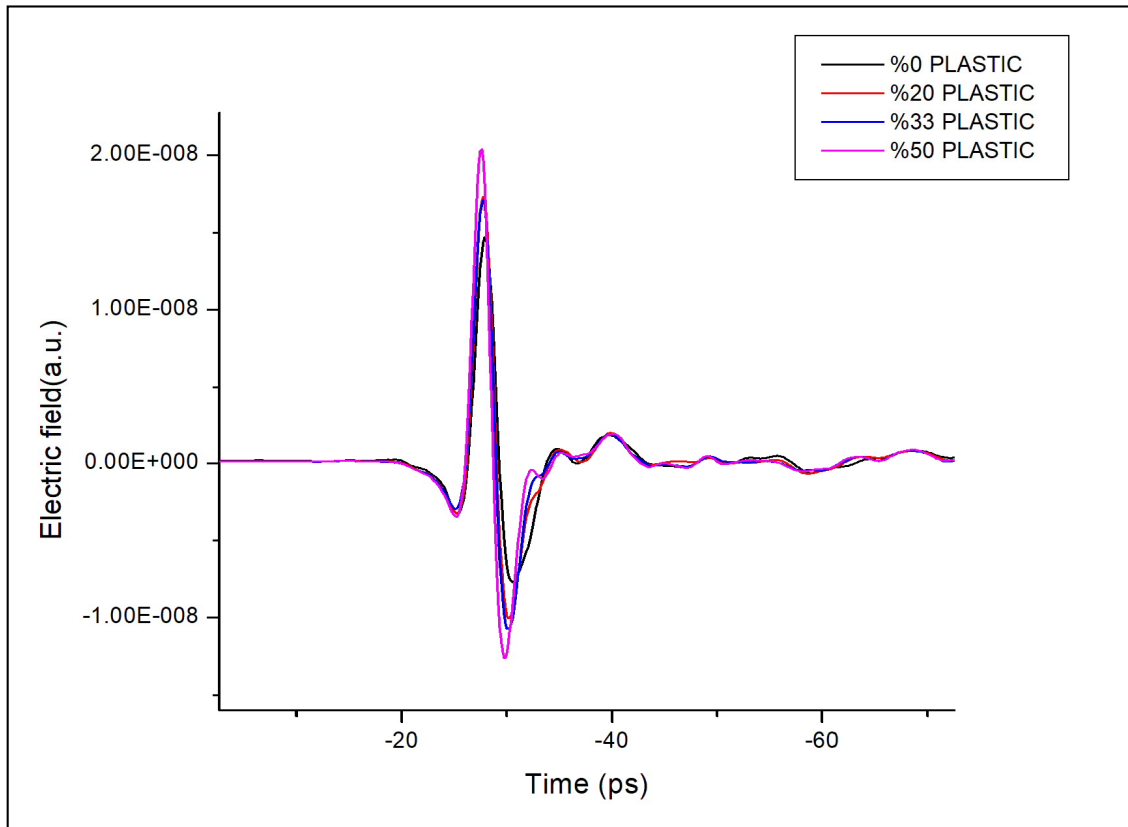


Figure 3.1 Samples THz-TDS

Figure 3.1 shows the THz time-domain pulse passing through the air and the samples. The samples are named 0%plastic, 20%plastic, 33%plastic and 50%plastic, respectively.

In general, food has some water in it, and the water existing in the food absorbs THz waves. Furthermore, the 0% sample, which contains only dog food, is expected to show less Electric Filed in THz-TD trace. As mentioned before in Chapter 2, THz waves are transparent when faced with plastic objects. In this experiment, the 50% plastic sample has more contaminants (plastic particles) than other samples. It is expected that the 50% plastic sample shows the highest electric field in the THz-TD trace. The 33% plastic sample contains a significant percentage of plastic relative to the reference (0% plastic sample), and the electric field is expected to show less than 50% plastic sample and more than 0% plastic sample. The 20%

plastic sample contains less percentage of contaminants and the electric field is expected to show less than 50% plastic sample and 33% plastic sample and more than 0% plastic sample. In Figure 3.1, the first spectrum (black), the 0%plastic sample, has the lowest electric field level at $1.00\text{E-}8$ a.u(This unit is the current from lock in amplifier and it is equal to 1nA), and the highest electric field level is the 50%plastic sample (purple spectrum) at $2.00\text{E-}8$ a.u. Two more samples, 33% plastic sample and 20% plastic sample, are strictly between 0%plastic sample and 50% plastic sample, which is correct. However, not in the order expected. The following Figure 3.2 shows a zoomed image of Figure 3.1.

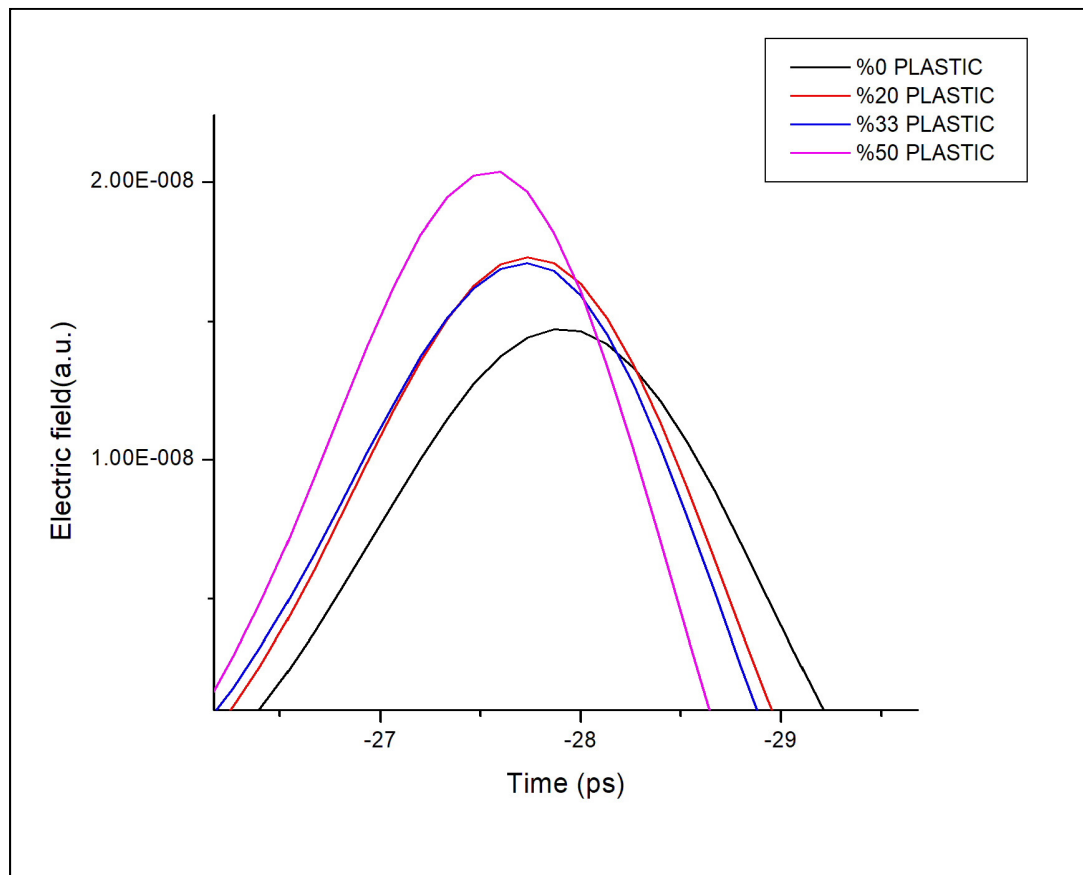


Figure 3.2 Time-domain spectra of samples zoom image

As mentioned in Chapter Two, Dry media such as paper, cloth, and plastic are transparent to THz radiation. Therefore with the increase the amount of plastic in each sample, it is expected that the amplitude (a.u) will become higher than before (see Figure 3.3 and 3.4).

The THz frequency domain results shows that the setup works well for 0% plastic and 50% plastic; however, for 20% plastic and 33% plastic, due to the high THz dispersion, it was not able to correctly detect the difference of contaminants. Another reason we could not see the difference is that the system was not sensitive enough, and we have a certain margin of error that is too high to differentiate the 20 and 33% sample. As a result, both give more or less the same result. Nevertheless, they are sandwiched between 0 and 50%, which is a constant results. Furthermore, The frequency range between 0.2 to 0.45 is more sensitive to the changes in plastic percentage.

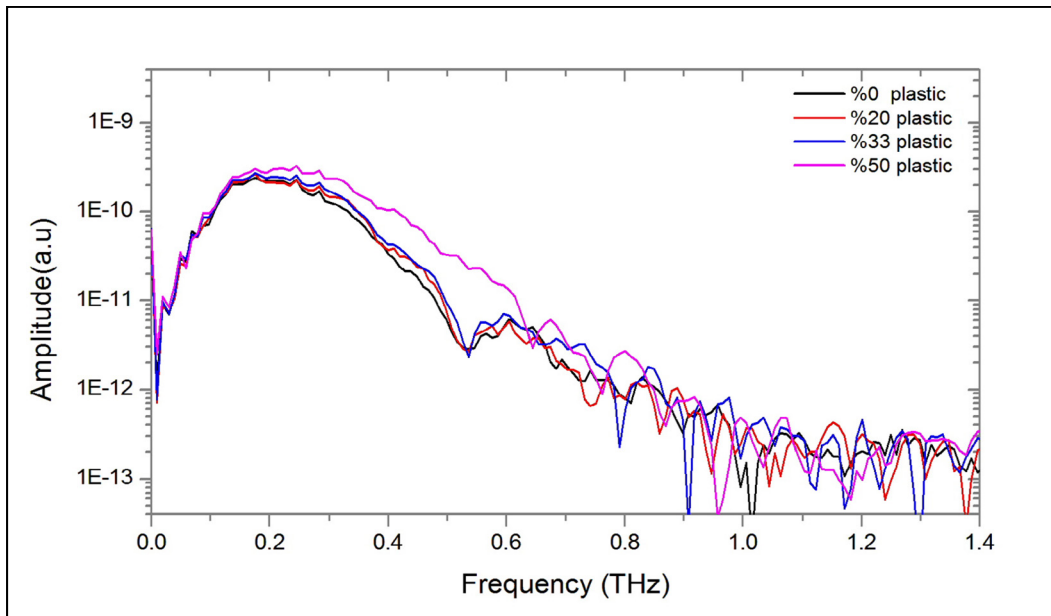


Figure 3.3 THz Frequency Domain

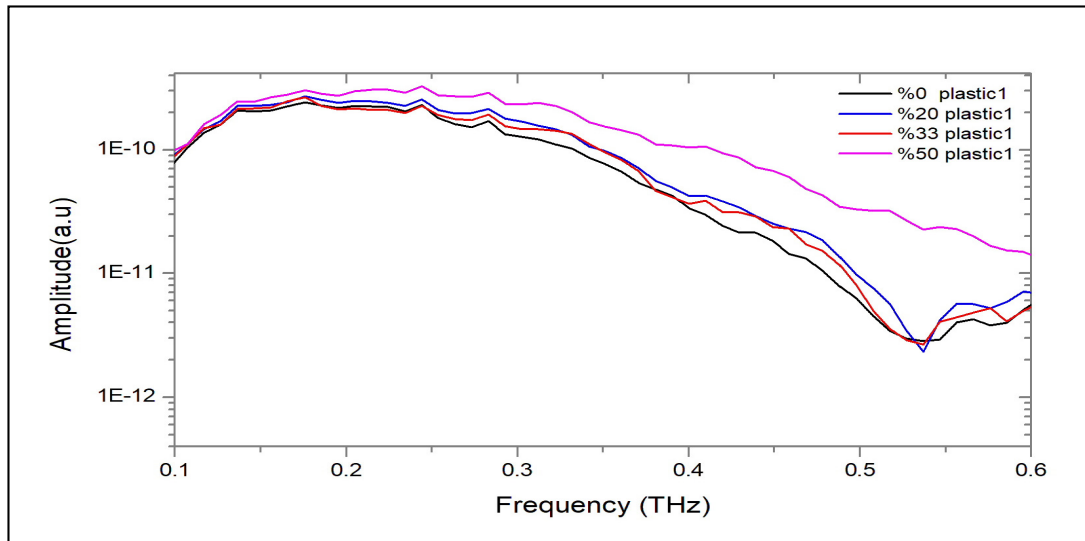


Figure 3.4 THz frequency domain zoomed image

Since the animal's food is in powder form, and powder creates scattered THz waves (Franz et al., 2008), a Teflon lens is used to collect more light. Therefore, a Teflon lens is added to the setup to collimate the dispersed light and find a signal properly upon detection (See Figure 2.8 b).

Here is a discussion of the results obtained by adding one lens before the detector (as depicted in Figure. 2.8(b)).

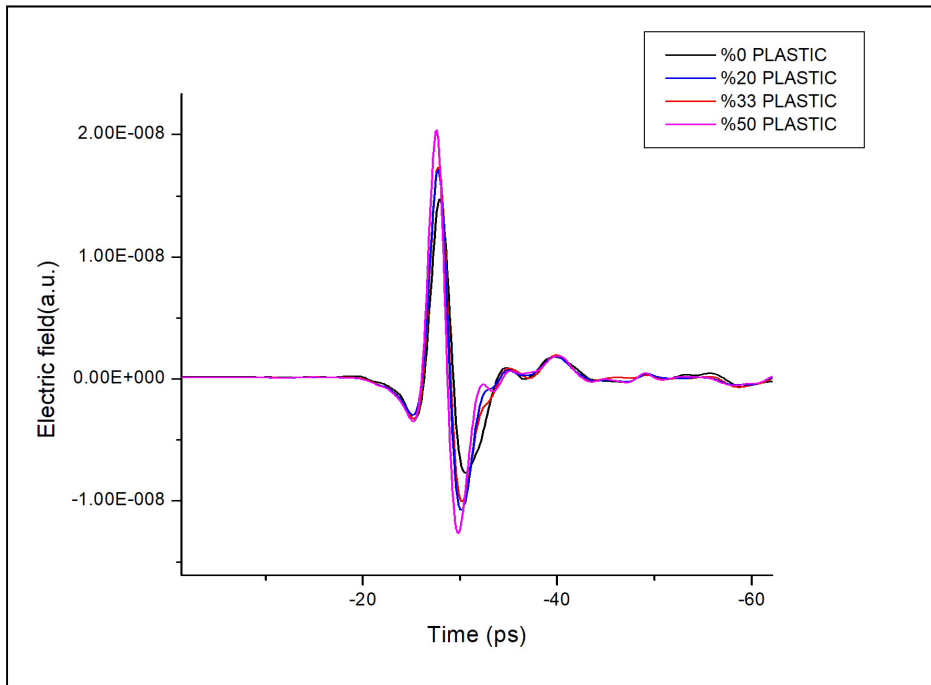


Figure 3.5 Time- Domain Spectra of samples when one lens add

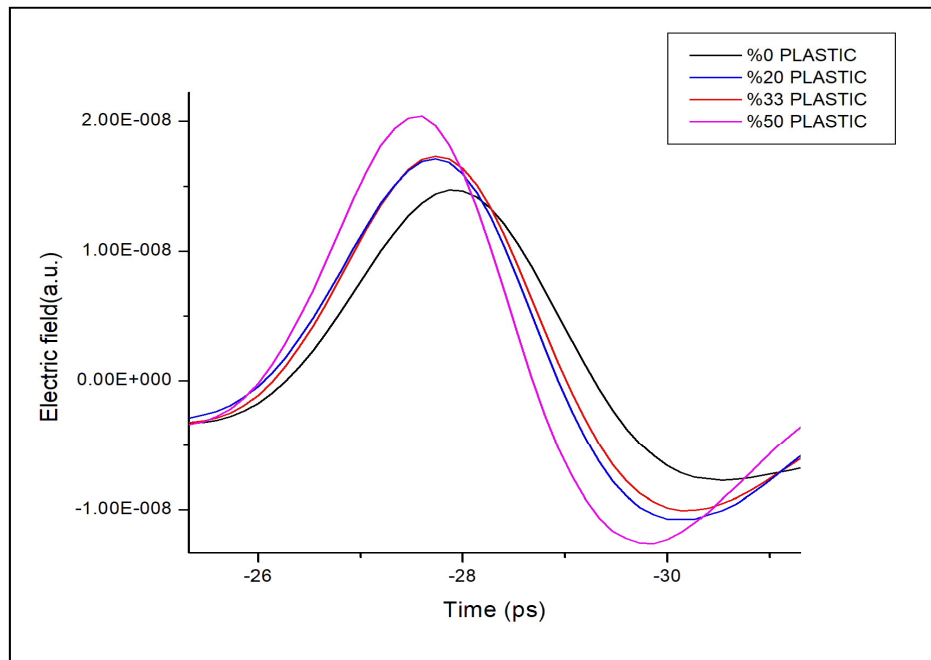


Figure 3.6 Zoomed image of Time-domain spectra of samples when the one lens add

As shown in Figure 3.5 and 3.6, after adding one lens to the setup, all spectra are enhanced and the differences between samples are apparent. The first temporal waveform (black) for 0% plastic sample, has the lowest peak electric field level at $1.460\text{E-}8$, and the highest electric field level is the 50%plastic sample (purple spectrum) at $2.00\text{E-}8$. The difference between 0% plastic and 20% plastic is noticeable. However, the difference between 20% plastic and 33% plastic is not completely obvious. (See Figure 3.7). Fourier transform information from these waveforms should be useful to reveal small differences observed in the time domain.

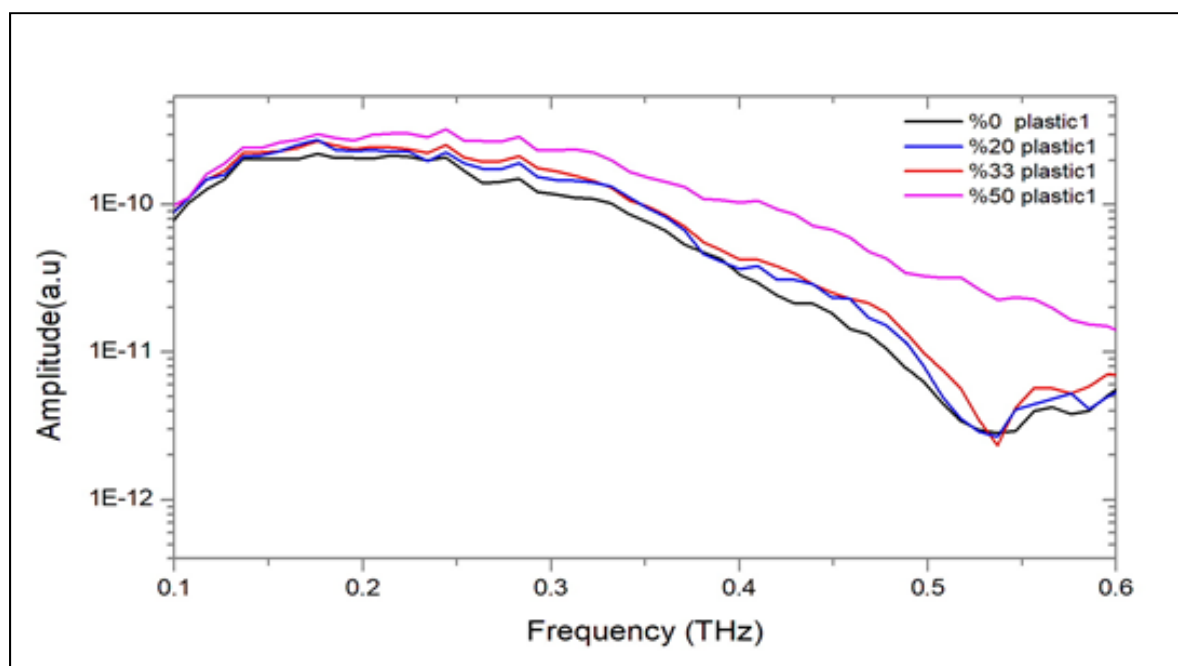


Figure 3.7 THz Frequency domain of samples when the one lens add

According to Figure 3.7, the difference between each sample is obtained in the frequency range from 0.2 THz to 0.3 THz. Although the 20% and 33% samples are very close to each other, they have still been correctly detected in terms of contaminants percentage. By focusing the

THz beam on the sample, we get a beam size of about 4 or 5 mm in diameter (with the one lens).

In order to more focus THz waves on the samples as well as recover the signal well for detection, the second lens is added to the setup. the second lens was added to the setup with this hypothesis. The following will review the results obtained from the third experiment.

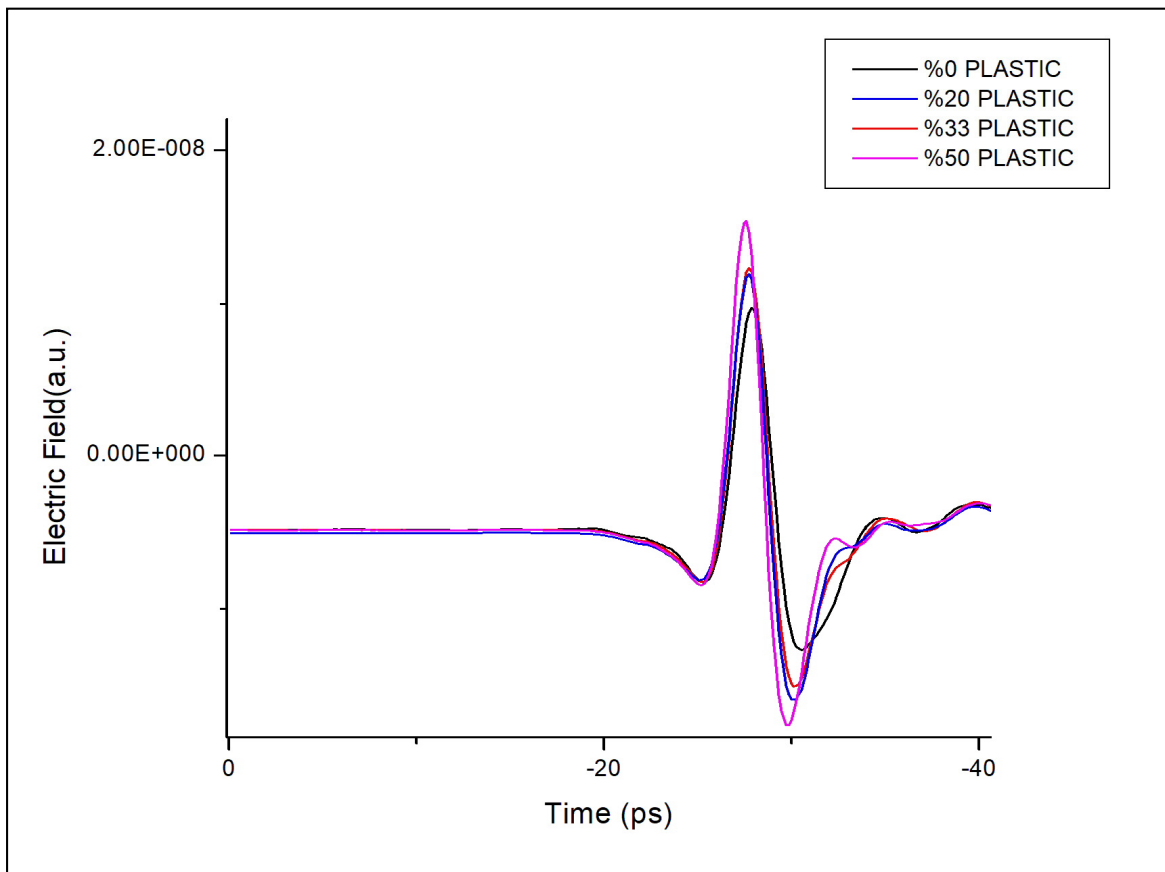


Figure 3.8 Time- Domain Spectra of samples when the two lenses add

After adding the second lens to the setup (as depicted in Figure. 2.8(c)), all spectra are improved and differences between samples are apparent completely. The first spectrum (black), the 0% plastic sample, has the lowest electric field level at $1.0700E-8$, and the highest

electric field level is the 50% plastic sample (purple spectrum) at $1.67.00E-8$. The difference between 20% plastic and 33% plastic is entirely noticeable. (See Figure 3.8 and 3.9).

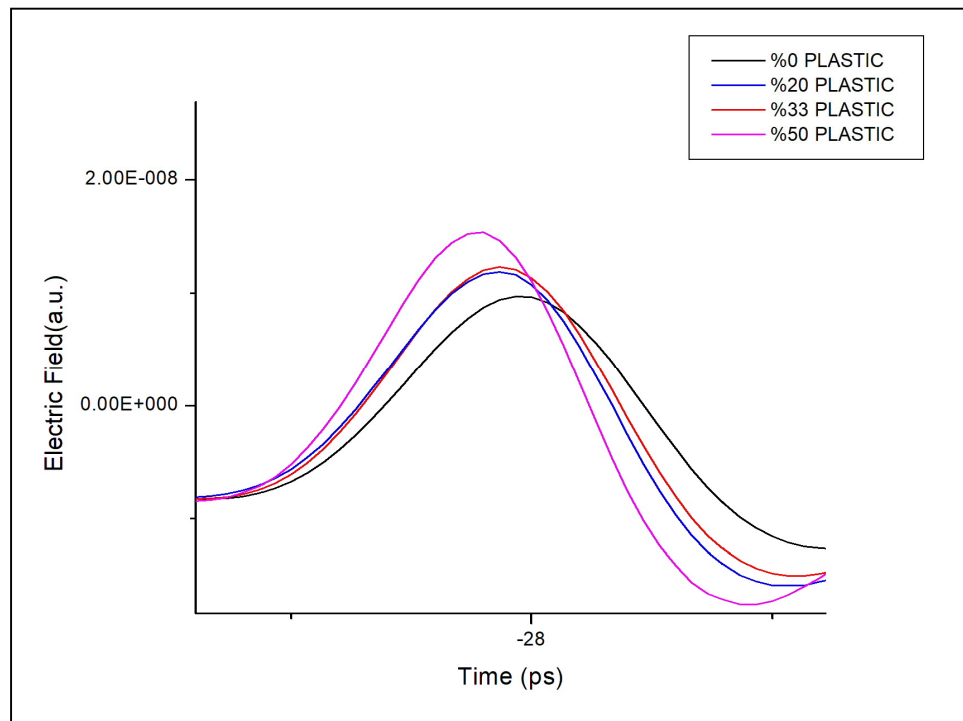


Figure 3.9 Zoomed image of Time-domain spectra of samples when the two lenses add

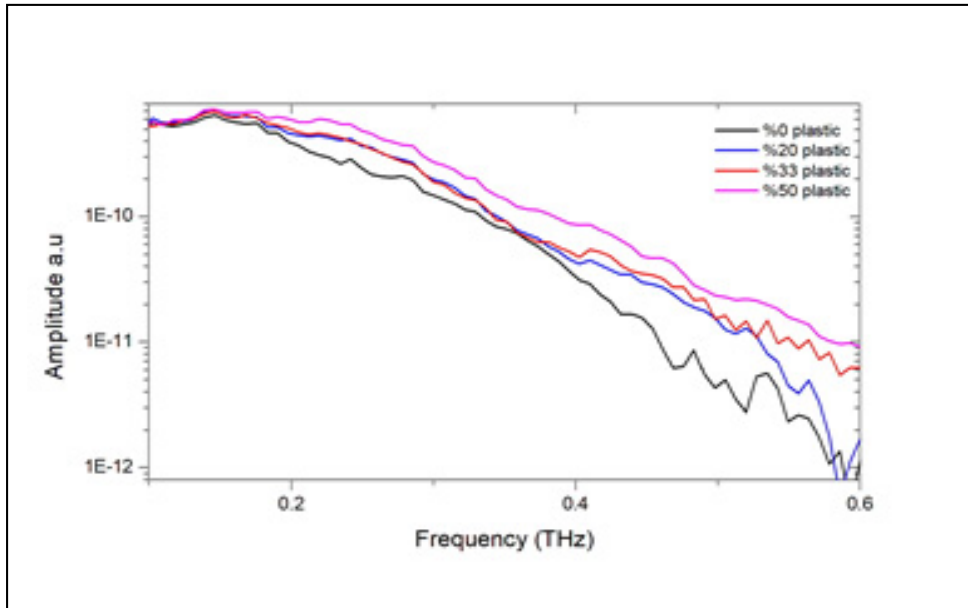


Figure 3.10 THz Frequency domain of samples when the two lenses added

The differentiation between 20% and 33% is still difficult to observe with our inspection system. However, the identification of the frequencies used for this type of inspection is quite clear. The frequency range between 0.2THz and 0.6 THz seems to be a good candidate for probing animal food powder (Figure 3.10)

3.3 Reflection spectroscopy and simulation results

THz reflection data were analyzed in the time domain to identify the internal structure of the samples, detect contaminants, and differentiate samples with and without plastic particles.

After several times redo the experiment, we couldn't succeed the same results as we get from transmission spectroscopy. Therefore we decide to do a reflection spectroscopy simulation.

As mentioned before, THz reflection spectroscopy of powder-sized particles was not possible with the existing system. In this thesis, the Finite-domain-time-difference (FDTD) software from Lumerical was used to simulate the particle behavior in reflection mode. For this purpose, a gold (Au) mirror with a thickness of 1 mm is used as a reference reflector. In front of this

mirror, there are four different sets of samples containing 3 particles of varying refractive index, as follows:

Sample 1: Include an Au (reflector) plus three particles with a 1.05 refractive index.

Sample 2: Include an Au (reflector) plus three particles with 1.05,1.1 and 1.05 refractive index.

Sample 3: Include an Au (reflector) plus three particles with 1.05,1.1 and 1.1 refractive index.

Sample 4: Include an Au (reflector) plus three particles with a 1.1 refractive index;

Figure 3.11 shows the simulation results. The black pulse represents the reference signal while the other 4 pulses correspond to the reflected beam after the 4 samples.

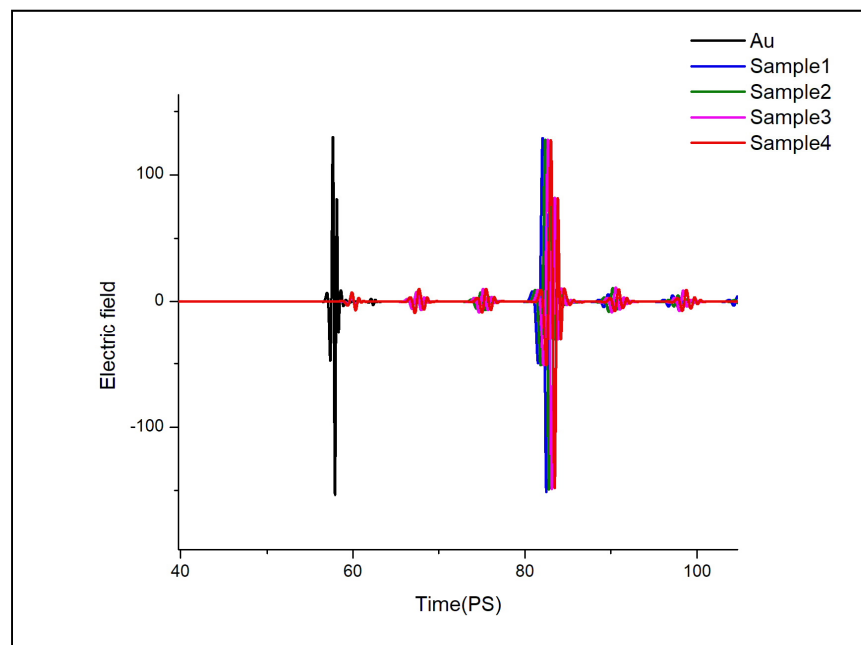


Figure 3.11 Different samples THz-TDS

The difference between the reference (black) and the samples is noticeable (Figure 3.11). However, the other samples are difficult to identify peak point and delay because they have a similar sort of refractive index. For more understanding, in Figure 3.12, sample 1 and sample

2 are plotted separately. As mentioned before, these two samples have different particles with different refractive indexes (sample 1: Include an Au (reflector) plus three particles with a 1.05 refractive index. And sample 2: Include an Au (reflector) plus three particles with 1.05, 1.1 and 1.05 refractive index). It is expected that by changing the refractive index to see a change in peak value and delay. After probing the results by THz-TD trace, it seems that these minor changes are not correctly visible only by using the THz-TD trace.

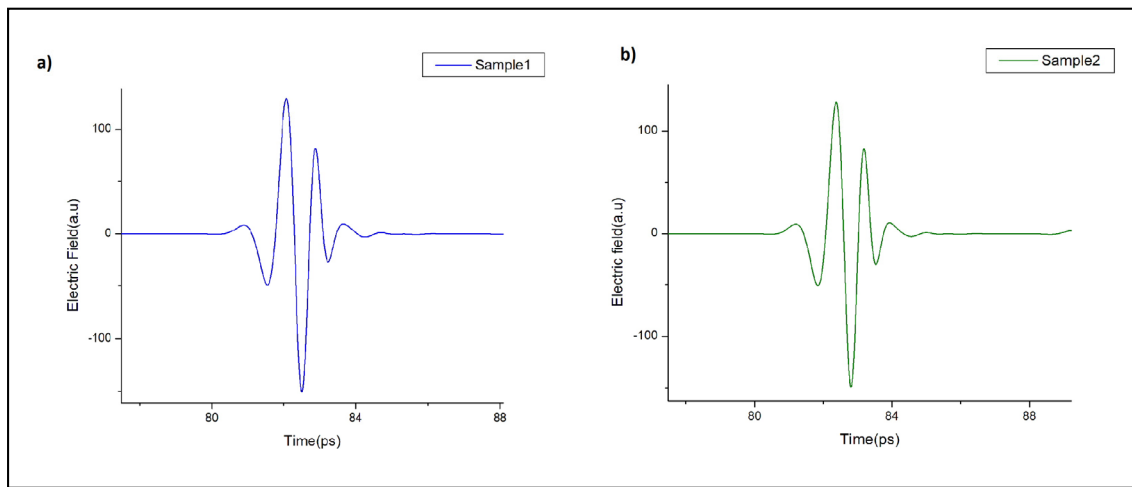


Figure 3.12 THz Time-Domain Spectroscopy of a) sample 1 and b) sample 2

Therefore, in order to identify each sample, wavelet analysis is used.. Matlab software is used to measure and plot the wavelet analysis. Therefore, the estimation of the spectral characteristics of a time series is time dependent. In the wavelet analysis, it is expected to find peak points and delay between each sample that it could not properly see in the THz-TD.

Figure 3.13 shows the wavelet analysis of sample 1. The bar to the right of figure shows the spectrum from blue at the lowest level to yellow at the highest level of the amplitude. With the help of this bar, we can find the amplitude peak point, which is yellow in this figure.

The maximum amplitude (a.u) is positioned between 80 ps to 84 ps and at the frequency of 0.982 THz.

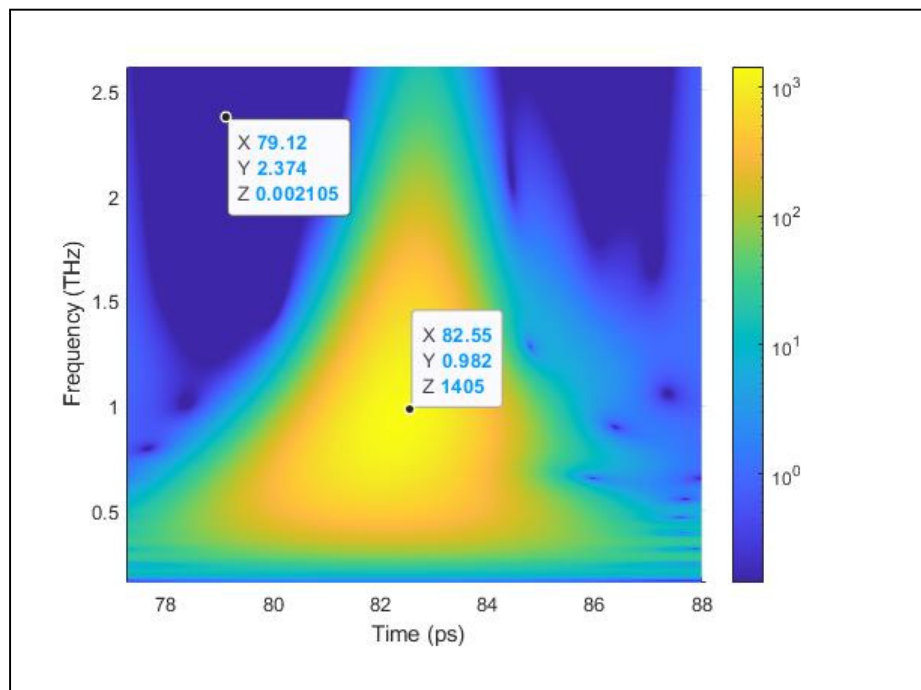


Figure 3.13 Sample 1 wavelet analysis

Figure 3.14 shows the wavelet analysis of sample 2. In the range of 81 ps to 84 ps and at the frequency of 0.9624 THz, the highest value of the peak is noticeable. To compare with Figure 3.14, which is related to sample 1, the existence of delay between each set of sample can be apparent. However, no distinction is found between particles for each sample set.

This simulation experiment was a trial to learn Lumerical software and Wavelet analysis. Of course, more data are required to improve this demonstration. Other samples results are provided in APPENDIX II.

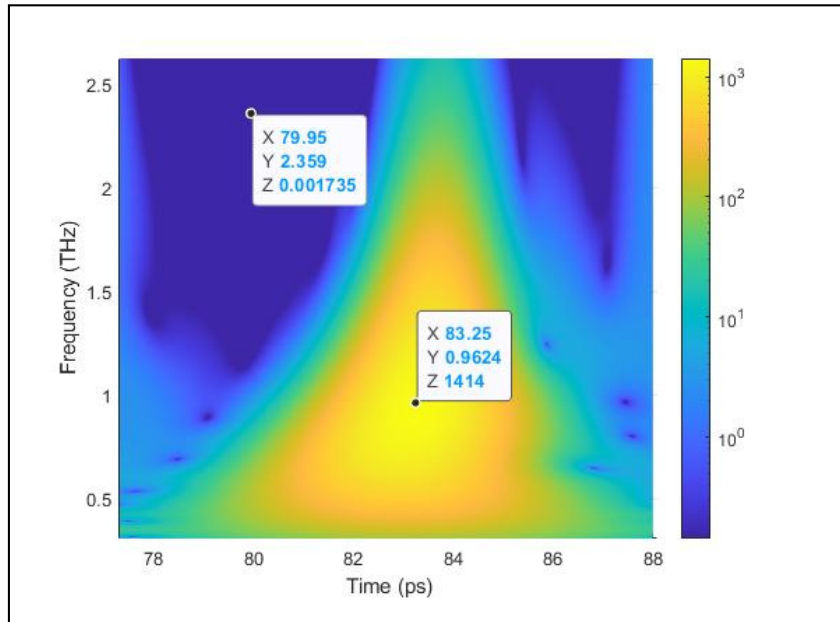


Figure 3.14 Sample 2 wavelet analysis

3.4 Polarizer quality control results

As mentioned in chapter two, we used a THz-TDS with measurement covering the frequency range of 0.2 -2.2 THz. Several scans of the polarizer were compared to determine the effective measurement range. If there was at least 97% agreement between scans at a specific frequency, this frequency is considered part of the effective measurement range and the effective polarization range (it means the frequency range for which the polarizer is polarising the light). This range was determined to be at least 0.2 to 1 THz for the polarizer.

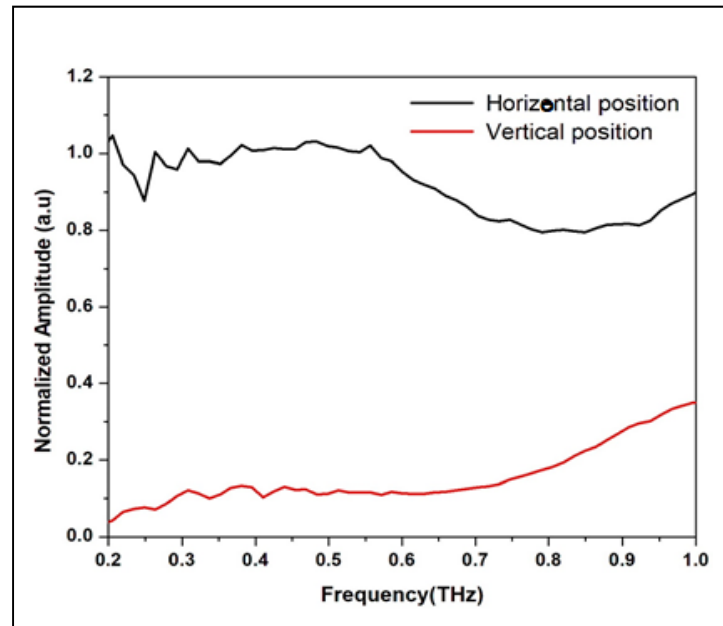


Figure 3.15 Horizontal and vertical polarizer position normalized amplitude

When the polarizer is in the vertical position with vertically polarized THz waves, the electric field is reflected from the polarizer, as shown by the normalized transmission (red curve). The black curve shows the normalized transmission for the THz field polarized perpendicular to the bar orientation with maximum transmission, as expected (See Figure3.15).

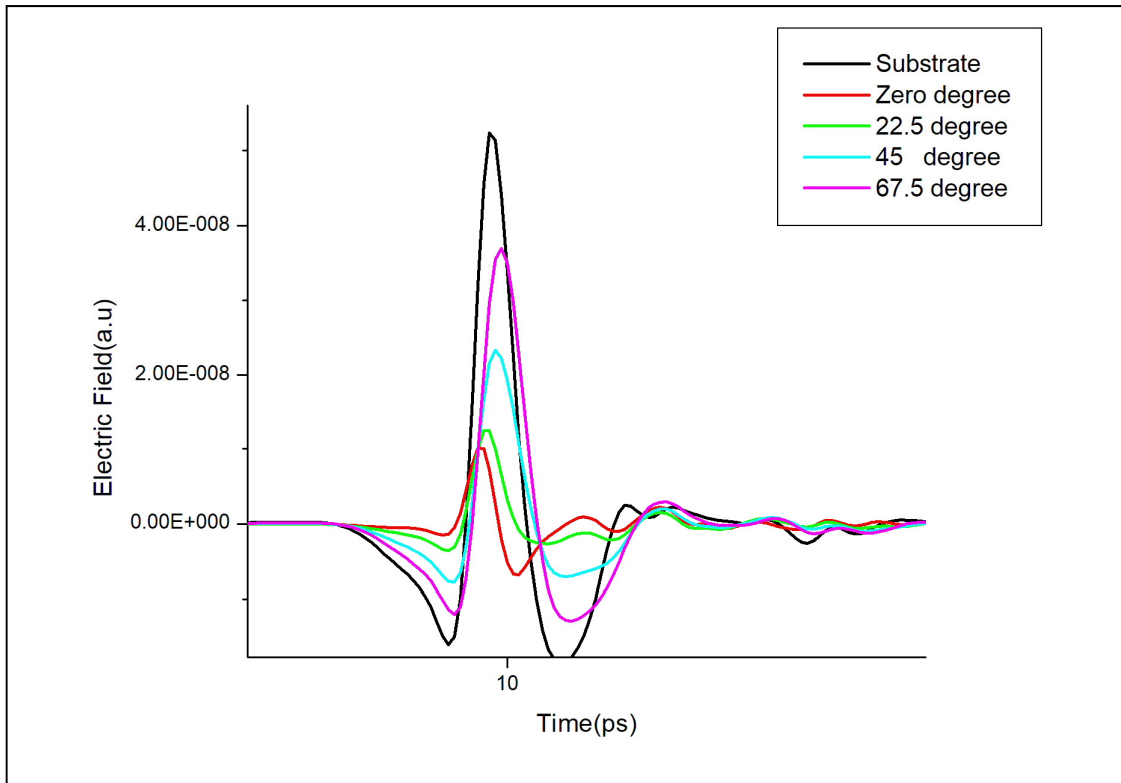


Figure 3.16 THz-TDS of polarizer in different positions

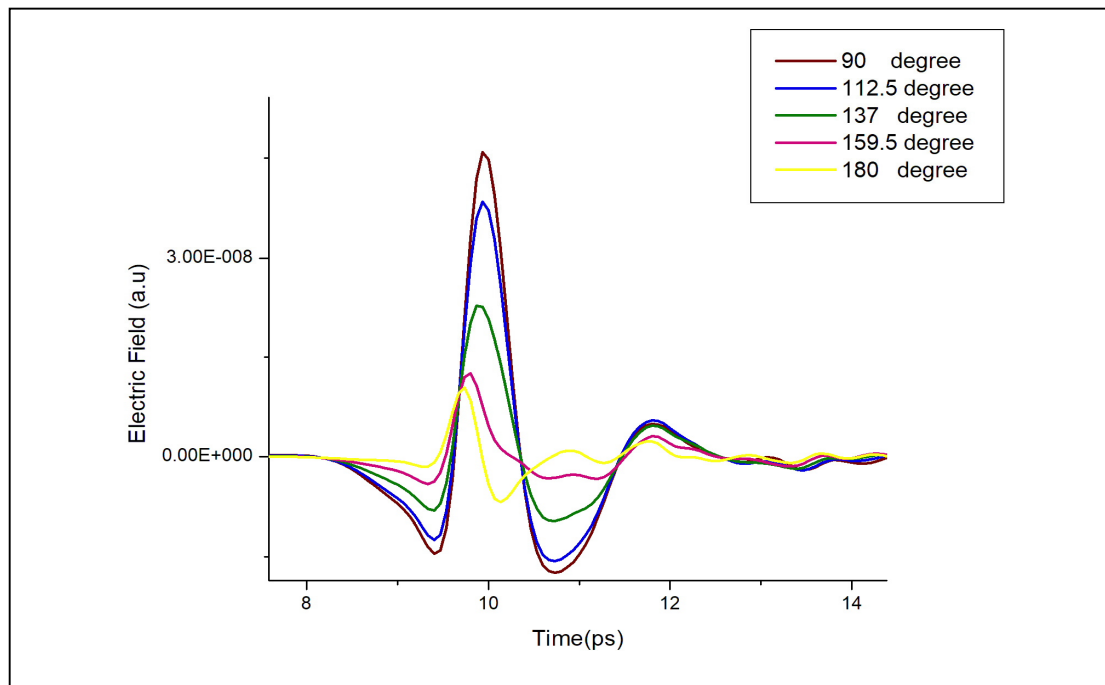


Figure 3.17 THz-TDS of polarizer in different positions

In order to accurately measure the quality of the polarizer, it was examined at different degrees. Figure 3.18 and 3.19 shows the THz-TDS of different degrees of polarization. The results clearly show that degrees zero and 180 are identical and have the lowest peak. Similarly, degrees 22.5 and 159.5, 45 and 137 and 67.5 and 112.5 are identical and 90 degrees shows highest peak.

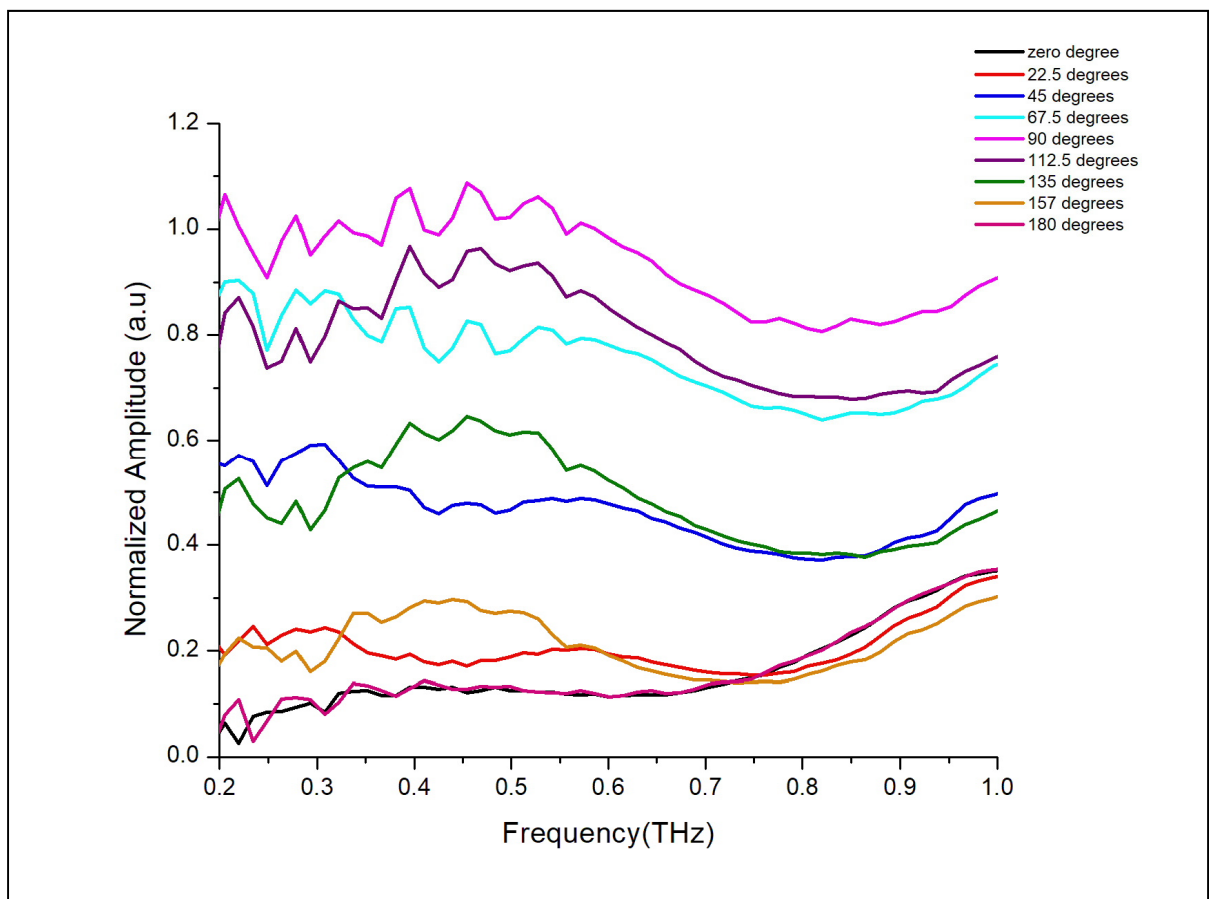


Figure 3.18 Different polarizer position normalized amplitude

The results obtained from the normalized amplitude in the THz frequency range (see Figure 3.18) show the highest amplitude of 90 degrees at 1.03. The normalized amplitude for degree zero and degree 180 is completely the same and shows the lowest amplitude. The other symmetrical degrees support each other, which is the critical result.

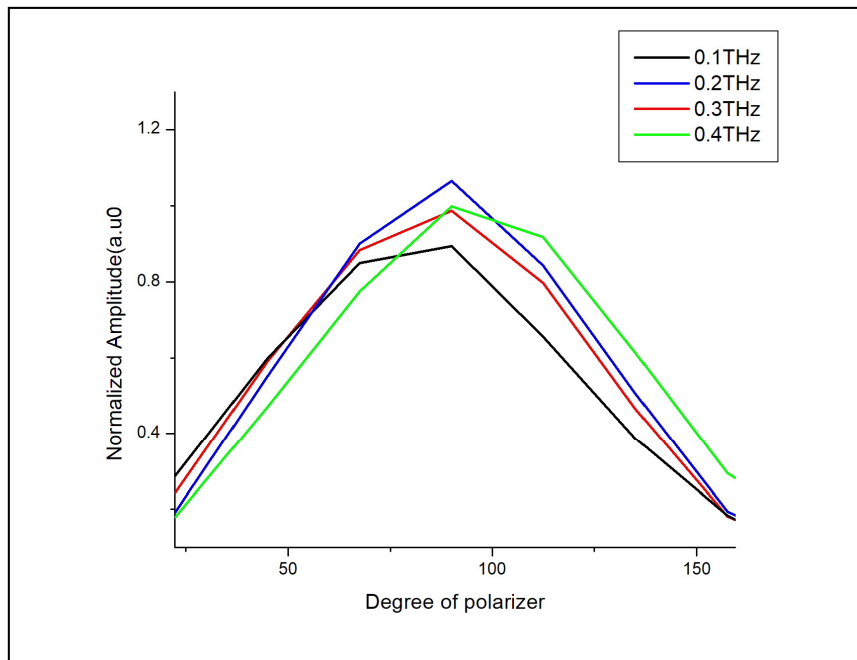


Figure 3.19 Normalized amplitude as a function of angels

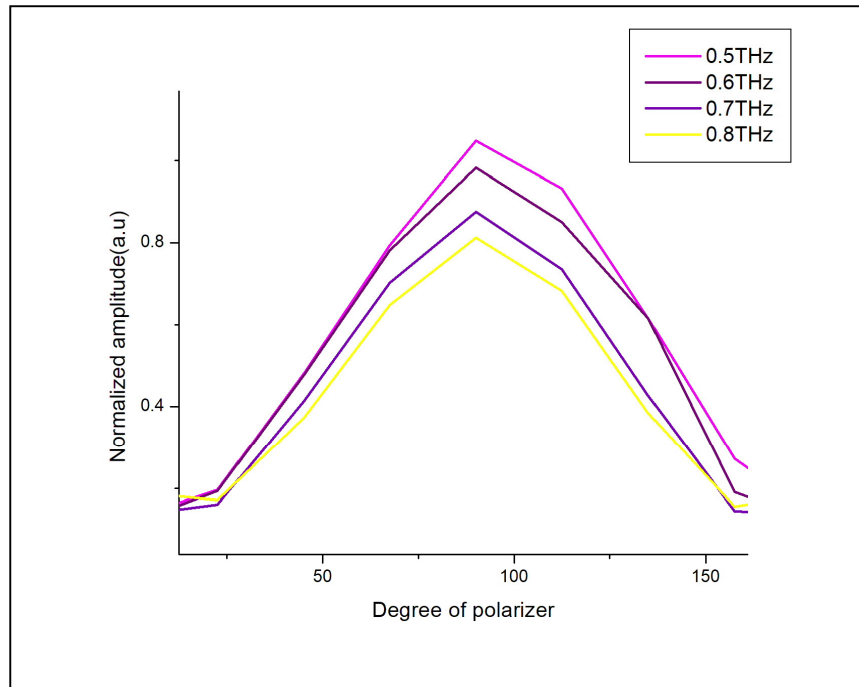


Figure 3.20 Normalized amplitude as a function of angles

Figure 3.19 and 3.20 illustrates; each samples shows a same peak at 90 degree. it is expected to see a sinusoidal function. this experiment done for the half rotation and the results are meet the expectations and clearly show that a PE polariser is well-suited for frequency operation below 1 THz.

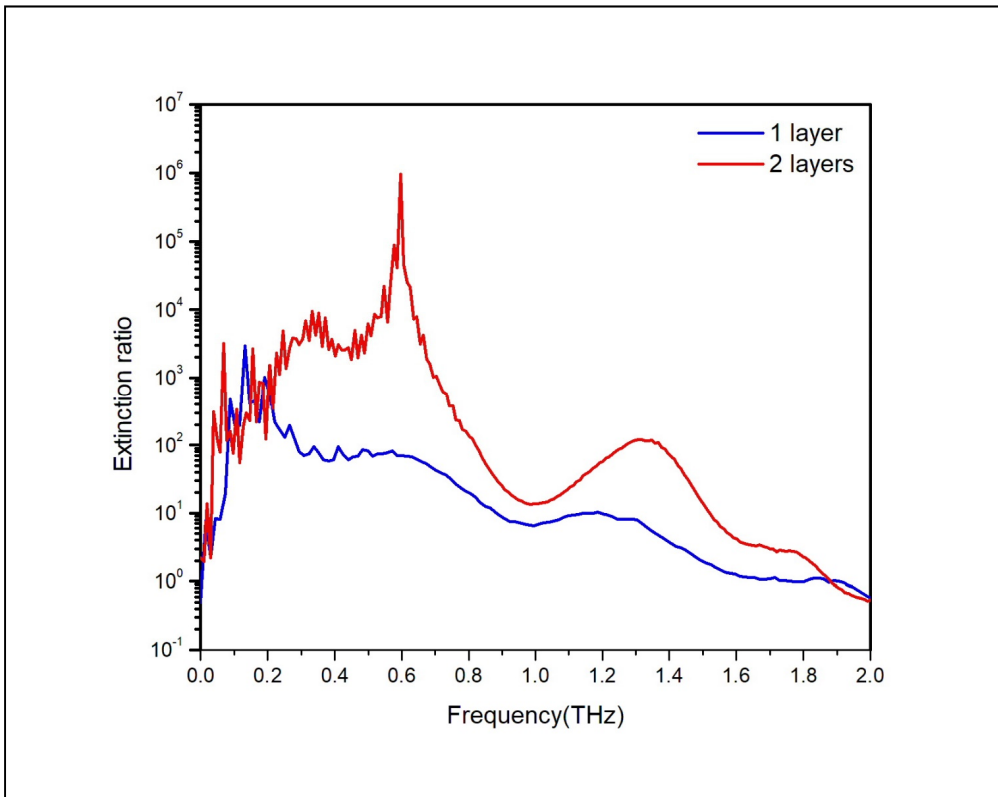


Figure 3.21 One layer polarizer and two layer polarizer extinction ratio

The Extinction ratio is defined as the maximum power transmission (electric field polarized perpendicular to the printed lines) over the minimum power transmission (electric field polarized parallel to the printed lines). Note that the polarizer performs better at low frequencies with a higher extinction ratio. However, for frequency below 0.2 THz, is obtained a lower extinction ratio than at 0.4 THz. (see Figure3.21)

The ink thickness of 352 nm is not sufficient (i.e., less than the skin depth) to reflect these frequencies well. Skin Depth refers to how deeply a signal can penetrate a material, which is dependent on the frequency as well as the material's properties. In this case, we could evaluated the skin-depth value for the printed silver ink, which is defined by:

$$\delta = 1/\sqrt{\pi f \mu_0 \sigma_{dc}} \quad (3.1)$$

Where the skin-depth is defined at the frequency f , with μ_0 is the vacuum permeability, and σ_{dc} is the dc conductivity of the material, which was 4.40×10^6 S/m for printed ink (Figure 3.22). (M Zhuldybina et al., 2021).

Fortunately, the addition of a second polarizer corrects much of this problem (see red curve). Stacking two printed devices artificially increases the thickness of the metal layer which allow us to exceed a skin depth at 0.2 THz

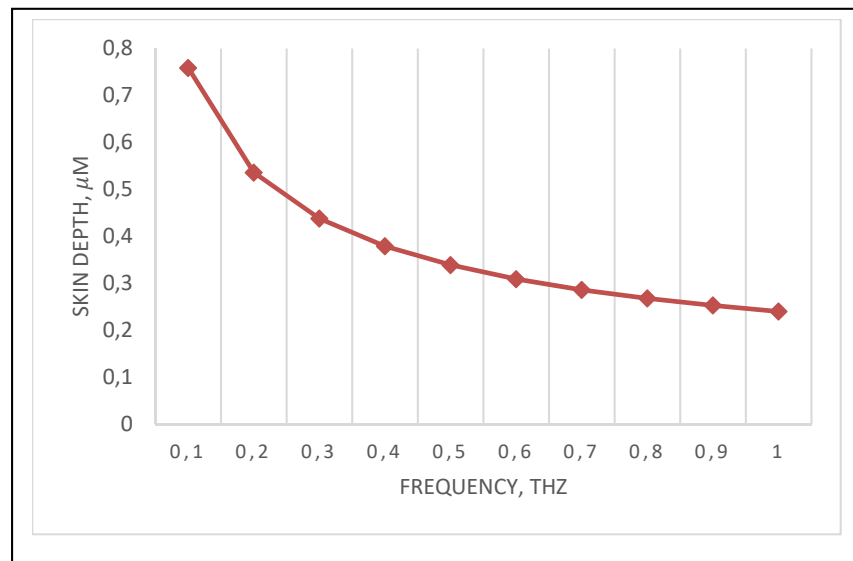


Figure 3.22 The skin depth evaluation as a frequency function

CONCLUSION AND RECOMMENDATIONS

This research aimed to use THz-TDS in quality control. In both experiments, feed quality control and polarizer quality control, to analyze the quality of the samples studied, we used a conventional THz-TDS with two PCA as transmitter and detector in transmission mode. The PCAs were pumped with a Ti: Sapphire laser oscillator providing 810 nm, 40 fs laser pulses at a repetition rate of 80 MHz and an average power of 20 mW on each antenna. The transmitter generates a vertically polarized THz beam. The detector receives the THz pulse, which has passed through the samples.

The most important challenges of this research project were contaminant detection and identification of differentiated samples with and without plastic particles for food quality control. The variable quality of the samples, due to heterogeneous, complex, uneven surfaces and sample tilt, affected the measurements, scans and spectra of the THz system, increasing scattering effects. We therefore tried to find solutions to avoid all these undesirable problems.

The food quality control analysis results showed that using two Teflon lenses in the design was the right solution. The results showed better sensitivity, dynamic range, and contaminant discrimination. This information is critical as it confirms that THz lenses are necessary for this application.

We differentiated the signal between the 0% plastic sample and the sample containing 20% plastic volume. The differentiation between 20% and 33% plastic is difficult to observe with our inspection system. However, the identification of the frequencies that can be used for this type of inspection is quite clear. The frequency range between 200 and 450 GHz seems to be the perfect candidate for probing animal feed.

The use of a THz source operating in continuous mode (CW) rather than in pulsed mode would greatly increase the discrimination of these contaminants.

The results of the second research project showed that we characterized the polarization capability in the THz frequency range of new polarizers fabricated from the silver ink (NovaCentrix PFI600) printed on the PET substrate (125 μm thick) at the production speed of 15 m/min.

We found that the polarizer topology consisting of lines with a spacing of 50 μm and a width of 50 μm is very effective in the frequency range of 0.2-1.0 THz.

By examining the results obtained from normalized amplitude, all symmetrical degrees support each other, which is the critical result.

Additional stacking of these polarizers could demonstrate ultimate polarization capability.

APPENDIX I

SAMPLE HOLDER

Figure A-I-1 shows the sample holder design detail in AutoCAD software with the all sizes. As presented earlier the sample holder is used to fix the sample and prepare that for the measurements. The hole inside the sample holder created to put the specific screw inside that and fix that on top of stand which is connected to THz TDS setup.

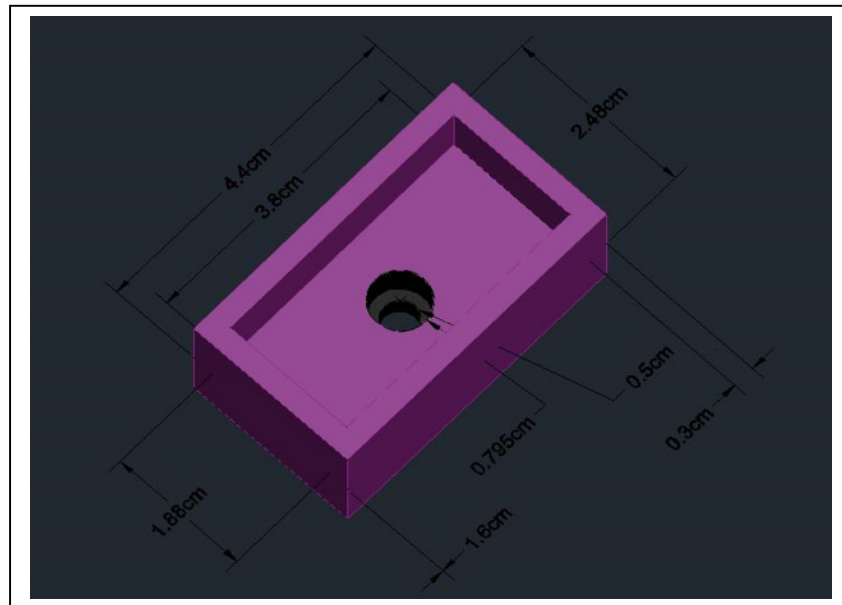


Figure-A I-1 Sample holder design detail

APPENDIX II

WAVELET ANALYSIS IN DIFFERENT SAMPLES

Figure A-II-1 and Figure A-II-2 show the wavelet analysis of samples 3 and 4. The bar to the right of figure shows the spectrum from blue at the lowest level to yellow at the highest level of the magnitude. With the help of this bar, we can find the intensity of the peak point, which is yellow in this figure.

The maximum peak for sample 3 is positioned in 81.5 to 84 (ps) and at the frequency of 0.953 THz. And The maximum peak for sample 4 is positioned in 81.5 to 84 (ps) and at the frequency of 0.9601 THz

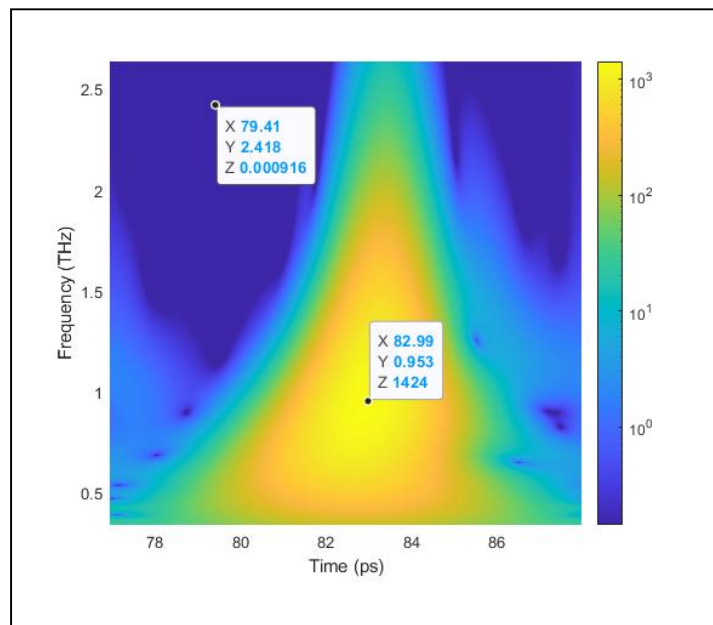


Figure A-II-1 Wavelet analysis of sample 3

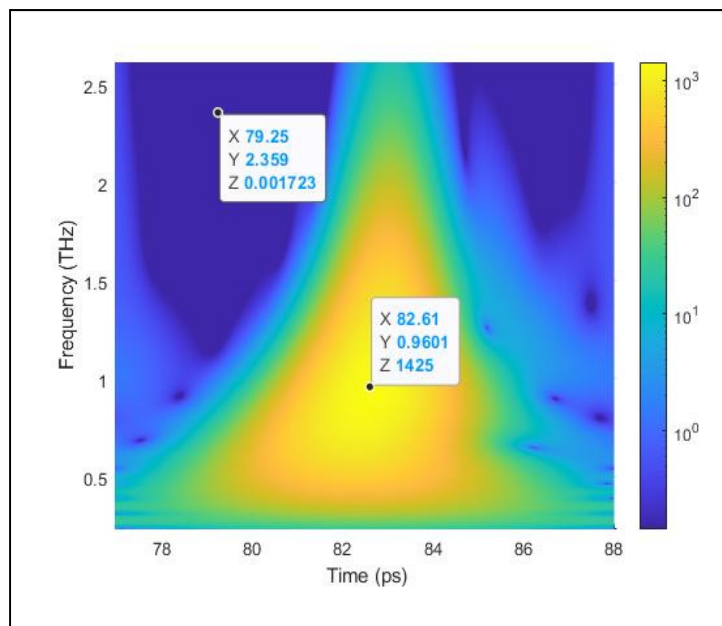


Figure A-II-2 Wavelet analysis of sample 4

BIBLIOGRAPHY

- Afsah-Hejri, L., Hajeb, P., Ara, P., & Ehsani, R. J. (2019). A comprehensive review on food applications of terahertz spectroscopy and imaging. *Comprehensive Reviews in Food Science and Food Safety*, 18(5), 1563-1621.
- Amarasinghe, Y., Zhang, W., Zhang, R., Mittleman, D. M., & Ma, J. (2020). Scattering of terahertz waves by snow. *Journal of Infrared, Millimeter, and Terahertz Waves*, 41(2), 215-224.
- Balocco, C., Kasjoo, S. R., Lu, X., Zhang, L., Alimi, Y., Winnerl, S., . . . Song, A. M. (2010). Novel terahertz nanodevices and circuits. Dans *2010 10th IEEE International Conference on Solid-State and Integrated Circuit Technology* (pp. 1176-1179). IEEE.
- Baxter, J. B., & Guglietta, G. W. (2011). Terahertz spectroscopy. *Analytical chemistry*, 83(12), 4342-4368.
- Cook, B. S., Fang, Y., Kim, S., Le, T., Goodwin, W. B., Sandhage, K. H., & Tentzeris, M. M. (2013). Inkjet catalyst printing and electroless copper deposition for low-cost patterned microwave passive devices on paper. *Electronic Materials Letters*, 9(5), 669-676.
- Davies, G., & Linfield, E. (2004). Bridging the terahertz gap. *Physics world*, 17(4), 37.
- Dexheimer, S. L. (2007). Coherent Vibrational Dynamics of Exciton Self-Trapping in Quasi-One-Dimensional Systems. Dans *Coherent Vibrational Dynamics* (pp. 239-270). CRC Press.
- Fan, S., Li, T., Zhou, J., Liu, X., Liu, X., Qi, H., & Mu, Z. (2017). Terahertz non-destructive imaging of cracks and cracking in structures of cement-based materials. *AIP Advances*, 7(11), 115202.
- Federici, J., & Moeller, L. (2010). Review of terahertz and subterahertz wireless communications. *Journal of applied physics*, 107(11), 6.
- Federici, J. F., Schulkin, B., Huang, F., Gary, D., Barat, R., Oliveira, F., & Zimdars, D. (2005). THz imaging and sensing for security applications—explosives, weapons and drugs. *Semiconductor Science and Technology*, 20(7), S266.
- Franz, M., Fischer, B. M., & Walther, M. (2008). The Christiansen effect in terahertz time-domain spectra of coarse-grained powders. *Applied Physics Letters*, 92(2), 021107.
- Ge, H., Jiang, Y., Lian, F., Zhang, Y., & Xia, S. (2015). Characterization of wheat varieties using terahertz time-domain spectroscopy. *Sensors*, 15(6), 12560-12572.

- Ge, H., Jiang, Y., Xu, Z., Lian, F., Zhang, Y., & Xia, S. (2014). Identification of wheat quality using THz spectrum. *Optics Express*, 22(10), 12533-12544.
- Gowen, A. A., O'Sullivan, C., & O'Donnell, C. (2012). Terahertz time domain spectroscopy and imaging: Emerging techniques for food process monitoring and quality control. *Trends in Food Science & Technology*, 25(1), 40-46.
- Guerboukha, H., Nallappan, K., & Skorobogatiy, M. (2018). Toward real-time terahertz imaging. *Advances in Optics and Photonics*, 10(4), 843-938.
- Guiramand, L., Nkeck, J., Ropagnol, X., Ozaki, T., & Blanchard, F. (2022). Near-optimal intense and powerful terahertz source by optical rectification in lithium niobate crystal. *Photonics Research*, 10(2), 340-346.
- Hiromoto, N., Shiba, N., & Yamamoto, K. (2013). Detection of a human hair with polarization-dependent THz-time domain spectroscopy. Dans *2013 38th International Conference on Infrared, Millimeter, and Terahertz Waves (IRMMW-THz)* (pp. 1-2). IEEE.
- J. Hilton, D., P. Prasankumar, R., A. Trugman, S., J. Taylor, A., & D. Averitt, R. (2006). On photo-induced phenomena in complex materials: probing quasiparticle dynamics using infrared and far-infrared pulses. *Journal of the Physical Society of Japan*, 75(1), 011006.
- Jansen, C., Wietzke, S., Peters, O., Scheller, M., Vieweg, N., Salhi, M., . . . Koch, M. (2010). Terahertz imaging: applications and perspectives. *Applied optics*, 49(19), E48-E57.
- Jepsen, P. U., Jacobsen, R. H., & Keiding, S. (1996). Generation and detection of terahertz pulses from biased semiconductor antennas. *JOSA B*, 13(11), 2424-2436.
- Jin, B., Zhang, C., Wu, P., & Liu, S. (2010). Recent progress of terahertz spectroscopy on medicine and biology in China. *Terahertz Sci. Technol.*, 3(4), 192-200.
- Massaouti, M., Daskalaki, C., Gorodetsky, A., Koulouklidis, A. D., & Tzortzakis, S. (2013). Detection of harmful residues in honey using terahertz time-domain spectroscopy. *Applied spectroscopy*, 67(11), 1264-1269.
- McIntosh, A. I., Yang, B., Goldup, S. M., Watkinson, M., & Donnan, R. S. (2012). Terahertz spectroscopy: a powerful new tool for the chemical sciences? *Chemical Society Reviews*, 41(6), 2072-2082.
- Münzenrieder, N., Shorubalko, I., Petti, L., Cantarella, G., Shkodra, B., Meister, T., . . . Tröster, G. (2020). Focused ion beam milling for the fabrication of 160 nm channel length IGZO TFTs on flexible polymer substrates. *Flexible and Printed Electronics*, 5(1), 015007.

- Nallappan, K., Dash, J., Ray, S., & Pesala, B. (2013). Identification of adulterants in turmeric powder using terahertz spectroscopy. Dans *2013 38th International Conference on Infrared, Millimeter, and Terahertz Waves (IRMMW-THz)* (pp. 1-2). IEEE.
- Ogawa, Y., Hayashi, S. i., Kondo, N., Ninomiya, K., Otani, C., & Kawase, K. (2006). Feasibility on the quality evaluation of agricultural products with terahertz electromagnetic wave. Dans *2006 ASAE Annual Meeting* (pp. 1). American Society of Agricultural and Biological Engineers.
- Palka, N., Szustakowski, M., Kowalski, M., Trzcinski, T., Ryniec, R., Piszczek, M., . . . Wrobel, J. (2012). THz spectroscopy and imaging in security applications. Dans *2012 19th International Conference on Microwaves, Radar & Wireless Communications* (Vol. 1, pp. 265-270). IEEE.
- Pawar, A. Y., Sonawane, D. D., Erande, K. B., & Derle, D. V. (2013). Terahertz technology and its applications. *Drug invention today*, 5(2), 157-163.
- Peralta, X. G., Lipscomb, D., Wilmink, G. J., & Echchgadda, I. (2019). Terahertz spectroscopy of human skin tissue models with different melanin content. *Biomedical optics express*, 10(6), 2942-2955.
- Pradarutti, B., Müller, R., Freese, W., Matthäus, G., Riehemann, S., Notni, G., . . . Tünnermann, A. (2008). Terahertz line detection by a microlens array coupled photoconductive antenna array. *Optics Express*, 16(22), 18443-18450.
- Seung, H. K., Heng, P., Costas, P., Christine, K., Jean, M., & Dimos, P. (2007). All-inkjet-printed flexible electronics fabrication on a polymer substrate by low-temperature high-resolution selective laser sintering of metal nanoparticles. *Nanotechnology*, 18(34), 345202.
- Shan, J., Nahata, A., & Heinz, T. F. (2002). Terahertz time-domain spectroscopy based on nonlinear optics. *Journal of Nonlinear Optical Physics & Materials*, 11(01), 31-48.
- Shur, M. (2005). Terahertz technology: devices and applications. Dans *Proceedings of the 31st European Solid-State Circuits Conference, 2005. ESSCIRC 2005.* (pp. 13-21). IEEE.
- Storm, K., Halvardsson, F., Heurlin, M., Lindgren, D., Gustafsson, A., Wu, P. M., . . . Samuelson, L. (2012). Spatially resolved Hall effect measurement in a single semiconductor nanowire. *Nature nanotechnology*, 7(11), 718-722.
- Swift, G. P. (2008). *Propagation of terahertz radiation in non-homogeneous materials and structures* (Durham University).

- Ueno, Y., Rungsawang, R., Tomita, I., & Ajito, K. (2006). Quantitative measurements of amino acids by terahertz time-domain transmission spectroscopy. *Analytical chemistry*, 78(15), 5424-5428.
- Van Exter, M., Fattering, C., & Grischkowsky, D. (1989). High-brightness terahertz beams characterized with an ultrafast detector. *Applied Physics Letters*, 55(4), 337-339.
- Venkataraman, S., Allison, D. P., Qi, H., Morrell-Falvey, J. L., Kallewaard, N., Crowe Jr, J. E., & Doktycz, M. J. (2006). Automated image analysis of atomic force microscopy images of rotavirus particles. *Ultramicroscopy*, 106(8-9), 829-837.
- Williams, G. P. (2005). Filling the THz gap—high power sources and applications. *Reports on Progress in Physics*, 69(2), 301.
- Yamaguchi, S., Fukushi, Y., Kubota, O., Itsuji, T., Ouchi, T., & Yamamoto, S. (2016). Brain tumor imaging of rat fresh tissue using terahertz spectroscopy. *Scientific reports*, 6(1), 1-6.
- Yan, Z., Ying, Y., Zhang, H., & Yu, H. (2006). Research progress of terahertz wave technology in food inspection. Dans *Terahertz Physics, Devices, and Systems* (Vol. 6373, pp. 63730R). International Society for Optics and Photonics.
- Yang, X., Yang, K., Luo, Y., & Fu, W. (2016). Terahertz spectroscopy for bacterial detection: opportunities and challenges. *Applied microbiology and biotechnology*, 100(12), 5289-5299.
- Zeng, Y., Edwards, M., Stevens, R., Bowen, J. W., Donnan, R. S., & Yang, B. (2017). Terahertz characterisation of UV offset lithographically printed electronic-ink. *Organic Electronics*, 48, 382-388.
- Zhang, H. Q., & Yan, Y. (2001). A wavelet-based approach to abrupt fault detection and diagnosis of sensors. *IEEE Transactions on Instrumentation and Measurement*, 50(5), 1389-1396.
- Zhong, S. (2019). Progress in terahertz nondestructive testing: A review. *Frontiers of Mechanical Engineering*, 14(3), 273-281.
- Zhuldybina, M., Béliveau, L.-P., Mansourian, M., Ropagnol, X., Trinh, N., Bois, C., & Blanchard, F. (2021). Mass-production of terahertz devices. Dans *2021 46th International Conference on Infrared, Millimeter and Terahertz Waves (IRMMW-THz)* (pp. 1-2). IEEE.

- Zhuldybina, M., Ropagnol, X., & Blanchard, F. (2021). Towards in-situ quality control of conductive printable electronics: a review of possible pathways. *Flexible and Printed Electronics*.
- Zhuldybina, M., Ropagnol, X., Bois, C., Zednik, R. J., & Blanchard, F. (2020). Printing accuracy tracking with 2D optical microscopy and super-resolution metamaterial-assisted 1D terahertz spectroscopy. *npj Flexible Electronics*, 4(1), 1-7.
- Zhuldybina, M., Ropagnol, X., Trudeau, C., Bolduc, M., Zednik, R. J., & Blanchard, F. (2019). Contactless in situ electrical characterization method of printed electronic devices with terahertz spectroscopy. *Sensors*, 19(3), 444.